Sources of black carbon at residential and traffic environments obtained by two source apportionment methods

Sanna Saarikoski[1], Jarkko V. Niemi[2], Minna Aurela[1], Liisa Pirjola[3,4], Anu Kousa[2], Topi Rönkkö[3], Hilkka Timonen[1]

[1]Atmospheric Composition Research, Finnish Meteorological Institute, Helsinki, FI-00101, Finland
[2]Helsinki Region Environmental Services Authority (HSY), Helsinki, FI-00066, Finland
[3]Aerosol Physics Laboratory, Physics Unit, Tampere University, Tampere, FI-33014, Finland
[4]Department of Automotive and Mechanical Engineering, Metropolia University of Applied Sciences, Vantaa, 01600, Finland

Correspondence to: Sanna Saarikoski (sanna.saarikoski@fmi.fi)

Abstract. This study investigated the sources of black carbon (BC) at two contrasting urban environments in Helsinki, Finland; residential area and street canyon. The measurement campaign at the residential area was conducted in winter-spring 2019 whereas the at the street canyon the measurements were carried out in autumn 2015. The sources of BC were explored by using positive matrix factorization (PMF) for the organic and refractory black carbon (rBC) mass spectra collected with a soot particle aerosol mass spectrometer (SP-AMS). Based on the PMF analysis, t~~T~~wo sites had different local BC sources; the largest fraction of BC originated from biomass burning at the residential site (38 %) and from the vehicular emissions at the street canyon (57 %). Also, the mass size distribution of BC diverged at the sites as BC from traffic was found at the particle size of ~100–150 nm whereas BC from biomass combustion was detected at ~300 nm. At both sites, a large fraction of BC was associated with urban background or long-range transported BC indicated by the high oxidation state of organics related to those PMF factors.

The results from the PMF analysis were compared with the source apportionment from the aethalometer model calculated with two pair of absorption Ångström values. It was found that several PMF factors can be attributed to wood combustion and fossil fuel fraction of BC provided by the aethalometer model. In general, the aethalometer model showed less variation between the sources within a day than PMF indicating that it was ~~being~~ less responsive to the fast changes in the BC sources at the site, or it could not distinguish between as many sources as PMF due to the similar optical properties of the BC sources.~~–~~ The results of this study increase understanding of the limitations and validity of the BC source apportionment methods in different environments. Moreover, this study advances the current knowledge of BC sources and especially the contribution of residential combustion in urban areas.

1 Introduction

Black carbon (BC) is a light-absorbing carbonaceous aerosol component that has significant climate impacts. It has a positive radiative forcing on climate (IPCC 2014), and when deposited on snow, it can lead to the reduction of the earth's surface albedo in snow-covered areas (Hansen & Nazarenko, 2004). Besides climatic effects, BC has been associated with adverse effects on public health in urban areas (Janssen et al. 2011; Segersson et al. 2017; WHO 2012). Atmospheric BC is characterized by a substantial spatial and temporal variation (Luoma et al., 2021) because of its unequally located sources and restricted atmospheric lifetime from days to weeks. Largest

BC concentration are typically measured in urban areas close to the source, however, BC can also be transported long distances with the air masses (Ikeda et al., 2017). Specially the transport of BC to Arctic areas has been associated with substantial impact on climate (AMAP, 2015).

BC is a primary particulate aerosol component that originates from incomplete combustion processes. It consists predominantly of agglomerated submicron particles (< 1µm), but shortly after emission, BC becomes mixed with other aerosol chemical species i.e. inorganics such as sulfate, nitrate and ammonium and organic compounds. In urban areas, the main sources of BC are typically transportation, residential combustion and industry (Bond et al., 2013). In recent years, BC emissions from vehicular traffic have been noticed to decrease due to technology advancements and legislation (Luoma et al., 2021; Pirjola et al., 2016; Järvinen et al., 2019), however, the regulation of residential combustion emissions is still in its infancy in many European countries (Klimont et al., 2017; Kukkonen et al., 2020). That trend may lead to the change in the BC source distribution by increasing the contribution of BC from residential combustion relative to the regulated source sectors i.e. engine and industrial emissions.

The sources of BC can be investigated with various methods. The origin of BC can be examined with statistical methods e.g. with positive matrix factorization (PMF; Paatero and Tapper, 1994; Paatero, 1997)~~. PMF~~ that is a receptor model that does not need a priori information on the profiles or time trends of the factors. PMF combined with an ~~However, PMF can produce a random number of factors, and therefore, it is up to the user to choose the solution that explains the data most accurately. This is commonly the most subjective stage of the analysis and depends largely on the skills of the PMF user (Engel-Cox and Weber, 2007).~~

Aerodyne aerosol mass spectrometer (AMS; Jayne et al., 2000) is a powerful tool to investigate the sources of submicron non-refractory particulate matter (e.g. Ulbrich et al., 2009), however, AMS equipped with ~~is one of the most advanced online instruments to explore the chemical constituents in particulate matter. The standard AMS is able to determine only non-refractory species, but by adding~~ a laser vaporizer ~~to the AMS~~ (soot particle aerosol mass spectrometer (SP-AMS); Onasch et al., 2012)~~, the range of determined species~~ can ~~be~~ extend the source apportionment~~ed~~ to refractory material such as refractory black carbon (rBC) and metals. ~~In terms of the PMF analysis for the refractory material, rBC and metal fragments are typically included in the mass spectra matrix of organics.~~ For example, Rivellini et al. (2020) found five sources for rBC, trace metals and organics in the ambient air of Singapore by applying PMF to the SP-AMS data while Bibi et al. (2020) utilized PMF to separate rBC originated from bonfires and domestic wood burning in UK. On the other hand, Saarikoski et al. (2019) have investigated the sources of rBC in an underground mine with PMF and Carbone et al. (2019) have distinguished fuel and lubricating oil related rBC in the diesel engine exhaust particles in the laboratory by using PMF for the mass spectra of rBC, organics and metals. One disadvantage of using PMF for the SP-AMS data is that the mass spectra of rBC contains relatively few fragments (typically largest signal observed for C_1^+ – C_5^+ fragments), and therefore, the identification of the sources is typically based on organic fragments. However, the rBC mass spectra has been noticed to be somewhat source specific differing for example for laboratory generated rBC particles and particles from aircraft turbine (Corbin et al., 2012), diesel truck and biomass burning particles (Onasch et al., 2015), and ambient hydrocarbon like organic aerosol (HOA) and oxygenated organic aerosol (OOA) factors (Rivellini et al., 2020). One option to improve the separation of BC sources is to include larger C_x fragments in the PMF matrix, as was done in the study of Bibi et al. (2020), where the addition of fullerenes signals (for example C_{60}^+) increased the number of meaningful sources.

~~Besides PMF, the sources of BC can be investigated by a chemical mass balance (CMB) model (Friedlander, 1973; Cooper and Watson 1980). It is also a receptor model, however, different from PMF, it requires a prior knowledge of the sources (source profiles) relevant to the measurement site. CMB has been used mostly for the filter samples, and therefore, instead of BC, the investigated component has been mostly elemental carbon (EC) determined by the thermal-optical methods. For example, Chen et al. (2012) found out that, out of eight investigated sources, diesel vehicles and hardwood burning in fireplaces and woodstoves emitted most of EC in Nevada US. Similar results have been obtained in the study of Yoon et al. (2018) which showed that the majority of EC was attributed to diesel vehicles and woodsmoke in San Francisco bay area.~~

The origin of BC can also be investigated by taking advantage of the absorption spectra of light-absorbing material in particles. BC is generally a powerful light absorber over the entire visible wavelength range. However, particles from fossil fuel and biomass combustion are characterized by different spectral dependencies, which allows to distinguish these sources based on their absorption properties. BC from fossil fuel combustion is assumed to absorb in the long visible and near infrared wavelengths (~600–950 nm) whereas other light-absorbing compounds, for example brown carbon from biomass burning, absorb light also close to the near ultraviolet and lower visible wavelengths (~300–500 nm; Kirchstetter et al., 2004; Laskin et al., 2015).

The source apportionment method based on the light absorption at~~in~~ different wavelengths is usually called an aethalometer model (Sandradewi et al., 2008a, 2008b; Herich et al., 2011¸ Wang et al., 2011a, 2011b) according to the multi-wavelength optical instrument typically used in the measurements. Aethalometer model assumes that the absorption from fossil fuel particles follows the spectral dependency of $\lambda^{-\alpha ff}$ and biomass combustion dependency of $\lambda^{-\alpha wb}$ in which the exponents are referred as absorption Ångström exponents (α) for fossil fuel (α_{ff}) and wood burning (α_{wb}). One of the largest sources of uncertainty in the aethalometer model is related to the selection of α_{ff} and α_{wb} values (Healy et al., 2017; Zotter et al., 2017) as the α values depend on the sampling site and selected wavelength range or pairs. It has been found that α_{ff} is typically in the range of ~0.8–1.2 in ambient air whereas α_{wb} can vary from 1.6 to 2.2 (Sandradewi et al., 2008b; Herich et al., 2011; Sciare et al., 2011; Zotter et al., 2017; Helin et al., 2018). It has also been shown that α values are affected by the core size of the BC particles, width of the size distribution and the chemical composition and thickness of the coating on the BC particles (Gyawali et al., 2009; Lack and Cappa, 2010; Lack and Langridge, 2013; Virkkula, 2020).

Besides PMF and aethalometer, the sources of BC can be investigated by a chemical mass balance (CMB) model (Friedlander, 1973; Cooper and Watson 1980), that is also a receptor model, however, different from PMF, it requires a prior knowledge of the sources (source profiles) relevant to the measurement site. Additionally, AMS PMF and aethalometer model are typically applied to the high time resolution data whereas CMB has been used mostly for the filter samples (Chen et al., 2012; Yoon et al., 2018). From the filter samples, the origin of BC can also be explored by analysing BC (or elemental carbon, EC) for radiocarbon ^{14}C. Measuring the ratio of ^{14}C to a stable carbon isotope, typically ^{12}C, provides information on the contributions of fossil and modern EC (e.g. in Szidat et al., 2004; Huang et al., 2006; Yttri et al., 2011).

~~The sources of BC have also been explored by analysing the filter samples for radiocarbon ^{14}C. 14C is present in living and contemporary plant materials, as it is transferred to plants by CO2 uptake, but it is absent in fossil fuels since it decays with a half-life of 5730 years. Hence, measuring the ratio of ^{14}C to a stable carbon isotope, typically ^{12}C, in EC provides information on the contributions of fossil and modern EC~~~~e.g. in Szidat et al. (2004), Huang~~

~~et al. (2006), Yttri et al. (2011) and Yoon et al. (2018)~~. ~~By combining ^{14}C analysis with e.g. analysis of levoglucosan, also biomass burning EC can be extracted. ^{14}C method for the source apportionment of EC has been used e.g. in Szidat et al. (2004), Huang et al. (2006), Yttri et al. (2011) and Yoon et al. (2018). ^{14}C analysis provides a highly accurate method to separate modern and fossil EC, however, as the EC concentrations are typically small compared to e.g. organic carbon concentrations, ^{14}C method typically requires a long collection time for the filter samples. Therefore, compared to the PMF and aethalometer models that can provide source apportionment on minute basis, ^{14}C method can give mean modern and fossil EC fractions for the several hours of averaged data.~~

The aim of this study was to investigate the sources of BC at two contrasting urban environments in Helsinki, Finland; residential area and street canyon. In this study, the sources of BC were explored by using PMF for the data collected with the SP-AMS. PMF analysis was applied to the organic data matrix that was complimented with three dominant refractory black carbon fragments; C_2^+, C_3^+ and C_4^+. The results from the PMF analysis were compared with the light absorption and source apportionment results from the multi-wavelength aethalometer. Although several studies have been published on the sources of BC in recent years, to our knowledge, this is the first time when the results from the PMF analysis have been compared with the results from the aethalometer model for BC at two measurement environments. Additionally, the emission factors for the biomass burning and traffic related BC were estimated at the residential site. This study utilized the state-of-the-art aerosol instruments and source apportionment tools to provide novel information on local, regional and remote sources of BC in Nordic urban environments. That data are highly required by the modelers and authorities when assessing the climate and air quality impact of BC as well as directing the emission legislation and emission mitigation actions.

2 Experimental methods

2.1 Measurement sites

2.1.1 Residential area

The measurements were conducted at the residential area in Pirkkola, Helsinki (Fig. S1), from 15 January to 16 April 2019. The measurement station was located in the middle of a detached housing area built primary in the 1940's, and it was operated by the Helsinki Region Environmental Services Authority (HSY). One of the main sources of particles in Pirkkola in cold season is wood burning. Unfortunately, there are no detailed statistics on wood burning in Pirkkola, but in general, fireplaces are used in ~80 % of detached and semi-detached houses in the Helsinki metropolitan area (Ohtonen et al., 2020), however, the use of biomass combustion as a primary heating source is scarce. Furthermore, many of the houses in Helsinki have a wood-heated sauna stoves (28 % of detached and semi-detached houses in the Helsinki metropolitan area on average). In addition to residential biomass burning, there was also some oil (light fuel oil) combustion in domestic boilers for the heating purposes in Pirkkola. In this study, we did not focus on oil burning as the emissions from heating oil burning did not impact BC concentrations (see Fig. ~~S1~~ S2 in supplemental material). Oil combustion affected CO_2 and NO concentrations with a minor influence also on particle number concentration (>5 nm particles; measured with CPC A20, Airmodus, Finland). Regarding traffic, there are some small and medium size streets (traffic volume of 3000–8000 vehicles per day; Statistics by the city of Helsinki) at the area that can have an influence on the pollutants measured at the site. Additionally, there are three busy roads within one kilometer radius from the site with the approximate traffic volumes of 124 000 (Ring road I; heavy duty 14 %), 67 000 (Highway E12; heavy duty 16 %) and 75 000 (Highway 45; heavy duty 16 %) vehicles per workday in 2019 (Statistics by the city of Helsinki). The Pirkkola site is described in more detail in Kuula et al. (2020).

2.1.1 Street canyon

The measurements at the street canyon were performed at the Mäkelänkatu Supersite (Fig. S1) between 2 and 22 October 2015. The SP-AMS measurements were not continuous at the street canyon site as they consisted of eight separate time periods with a total of 195 hours of data. The measurement station was located next to a six-lane street with an approximate traffic volume of 28 000 vehicles per workday (12 % of heavy duty) in 2015 (Statistics by the city of Helsinki). Major particle source at the site is traffic whereas the contribution of biomass burning to particle concentrations can be assumed to be minor since there are only very few small-house areas nearby. Also, the measurement period was in autumn when the need for the additional heating with wood was not notable (ambient temperature varied from -2 to 18 °C with an average of 7 °C in October 2015). Mäkelänkatu Supersite has been described in more detail in Hietikko et al. (2018) and Barreira et al. (~~2020~~2021). Besides local sources, long-range transport (LRT) from Central and Eastern Europe can have a significant impact on particle concentrations at all locations in the Helsinki area (e.g. in Niemi et al., 2009; Barreira et al., ~~2020~~2021).

2.2 Instruments

2.2.1 Soot Particle Aerosol Mass Spectrometer (SP-AMS)

The concentrations, mass spectra and size distributions of rBC were determined by the soot particle aerosol mass spectrometer (Aerodyne Research Inc, Billerica, US; Onasch et al., 2012). The SP-AMS is different from the standard AMS as it has an additional laser vaporizer that allows the determination of refractory particulate species. It is possible to operate the SP-AMS only with the laser vaporizer, however, both tungsten and laser vaporizers were utilized in this study in order to measure also all non-refractory particulate material i.e. organics, sulfate, nitrate, ammonium and chloride. Also the potassium signal was extracted from the data but it was used only for the validation of the PMF results. The SP-AMS size distributions were measured in a standard particle-time-of-flight (PToF) mode, and because of the aerodynamic lens in the SP-AMS, the size range was from ~50 nm to 1 µm. The SP-AMS was operated with a time-resolution of 90 and 30 sec at the residential and street canyon sites, respectively.

The SP-AMS data were analysed with IGOR 6.37 SQRL 1.62A and PIKA 1.22A softwares. ~~A collection efficiency of one was applied to both data sets.~~ Ionization efficiency for nitrate was determined by calibrating the instrument with ammonium nitrate while the relative ionization efficiency for rBC (0.05~~1~~) was based on the calibrations with Regal black. A collection efficiency of one was applied to both data sets.~~-~~ Compared to the aethalometer, rBC from the SP-AMS was consistently smaller than BC from the aethalometer (Fig. S3). Although the measurements in the SP-AMS and aethalometer are based on different techniques, the main reason for the lower rBC concentrations measured by the SP-AMS was likely to be the imperfect laser-to-particle beam alignment. Therefore, rBC from the SP-AMS data was normalized to the aethalometer BC concentrations that were assumed to represent total ambient BC more realistically.

The concentrations of non-refractory AMS species (organics, sulfate, ammonium, nitrate, chloride) were utilized in this study only for calculating the coating factor. In order to validate the non-refractory AMS concentrations, the sum of the SP-AMS species (excluding rBC) and BC from the aethalometer were compared with the concurrent PM_1 measurements (Grimm model EDM 180, Grimm Aerosol Technik, Ainring, Germany) at the residential site. The sum of the SP-AMS species and AE33 BC made on average 71% of Grimm PM_1 with a moderate correlation (Pearson's correlation coefficient $r = 0.888$; Fig. S4a). Similar comparison was done by using –the composition dependent collection efficiency (CDCE, Middlebrook et al., 2012) instead of constant CE=1. The time series of the CDCE are shown in Fig. S4c and Fig. S5 for both sites with the average CDCE being 0.59 and 0.49 for the residential and site street canyon sites, respectively. With the CDCE, the sum of the SP-AMS species and AE33 BC was closer to PM_1 from Grimm (~85% of PM_1), however, the correlation was slightly poorer ($r = 0.876$; Fig. S4b). For the street canyon site, PM_1 comparison could not be calculated as there was no PM_1 mass measurement at that time. The uncertainty in the coating factor due to the CE value of 1 will be discussed in Chapter 3.3.

2.2.2 Aethalometer (AE33)

Black carbon was measured optically by using a dual-spot aethalometer (AE33, Aerosol d.o.o., Ljubljana, Slovenia; Drinovec et al., 2015). AE33 operated with a flow rate of 5 L min^{-1} and a time resolution of one minute. Size cut at 1 µm was carried out by using a sharp cut cyclone (Model SCC1.197, BGI Inc., Butler, NJ, USA) in the inlet. The multiple scattering enhancement factor C of 1.57 was utilized (Drinovec et al., 2015) and the default mass absorption coefficient values were used. Since the aethalometer determined BC optically, it should be referred as equivalent BC (eBC), however, for the simplicity, it is called as BC in this paper.

2.2.3 Auxiliary measurement

24-hour PM_{10} filter samples were collected at both sites during the campaigns. PM_{10} samples were collected continuously at the residential site (a total of 89 samples), whereas at the street canyon, PM_{10} filters were collected every three days. PM_{10} filters were analyzed for biomass burning tracers, monosaccharide anhydrides (MAs) i.e. levoglucosan, mannosan and galactosan, with a liquid chromatograph mass spectrometer (Saarnio et al., 2010b). It should be noted here that, the MA results from the street canyon were not utilized in this study since the SP-AMS and PM_{10} sampling were not continuous at the street canyon and PM_{10} filter sampling overlapped the SP-AMS measurements only during short time periods. However, the average concentration of levoglucosan was 42 ng m^{-3} in PM_{10} in October 2015 at the street canyon. For the comparison, the average levoglucosan concentration at the residential site was more than double of that (110 ng m^{-3}) between 15 January and 16 April 2019.

The concentrations of nitrogen oxides (NO, NO_x and NO_2) were measured at the residential and street canyon sites with one-minute time-resolution (Horiba APNA 370, Kyoto, Japan). CO_2 was measured only at the residential site (1-minute time resolution; Vaisala GMP343, Vantaa, Finland). Regarding the meteorological parameters, only wind speed and wind direction were measured directly at the residential site. Ambient temperature data were taken from the Kumpula weather station that was located approximately five kilometres south-east from the residential site. The SP-AMS data from the street canyon were not analysed in terms of meteorology as the SP-AMS measurements were not continuous and the measurement period was rather limited. Both sites had also other air quality measurements such as $PM_{2.5}$ and PM_{10} but those results are not included in this paper.

BC concentrations at the residential site were compared with the concurrent measurements at the regional background air quality monitoring station (Luukki, Espoo; ~15 km northwest from residential site in Pirkkola, Fig. S1). BC at the Luukki site was measured with a multi angle absorption photometer (MAAP, model 5012, Thermo Fisher Scientific, Waltham, US) with one-minute time resolution. For the comparison of AE33 with MAAP (Chapter 3.1), BC from the AE33 was multiplied by a factor of 0.75 (Helin et al. 2018). All the other AE33 data are presented without the conversion factor.

2.3 Source apportionment

2.3.1 AMS PMF

The sources of BC were explored by analyzing the SP-AMS high-resolution (HR) mass spectra with PMF (CU AMS PMF tool v. 2.08D, Paatero and Tapper, 1994; Ulbrich et al., 2009). The data matrix contained organic fragments and three rBC fragments, C_2^+, C_3^+ and C_4^+. For the larger carbon fragments, the signal was close to the detection limit, and therefore, they were not included in the PMF analysis. The number of factors was varied from two to eight (Fig. ~~S2~~S6) of which the solutions with 3–5 factors were investigated in more detail. Before the PMF analyses, the SP-AMS data from the residential and street canyon sites were averaged to ten and five minutes, respectively. For the street canyon data, the CHO^+ fragment at mass-to-charge ratio (m/z) 29 was excluded from the data matrix. The reason for that was that N_2^+ at m/z 28 was fluctuating due to the unresolved issue in the instrument, which caused a large uncertainty for the determination of the isotope $^{15}NN^+$ at m/z 29 and also for CHO^+ that was overlapping $^{15}NN^+$.

The mass spectra, time series and diurnal trends for 3–5 factor PMF solutions are shown in Figs. ~~S3~~S7–S12~~8~~. For both sites, in three factor solutions the factors were identified as HOA, biomass burning organic aerosol (BBOA) and low-volatility OOA (LV-OOA). The mass spectra of HOA had a typical hydrocarbon pattern with the largest signals for $C_3H_5^+$, $C_3H_7^+$, $C_4H_7^+$, $C_4H_9^+$, $C_5H_9^+$ and $C_5H_{11}^+$ at m/z 41, 43, 55, 57, 69 and 71, respectively, and a large hydrogen-to-carbon ratio (H:C) and small oxygen-to-carbon ratio (O:C) for the organic fragments. At the residential site, HOA peaked during the morning rush hour at 9:00–10:00 and again later in the evening at 21:00–22:00. Similar morning peak was found for HOA at the street canyon, but the second maximum appeared earlier at 17:00–18:00 during the evening rush hour. The mass spectra of BBOA had the largest signal for oxygenated fragments $C_2H_4O_2^+$ and $C_3H_5O_2^+$ at m/z 60 and 73, respectively, that are typical fragments for the biomass burning emissions (Alfarra et al., 2007). In terms of diurnal trends, BBOA had the maximum between 20:00 and 21:00 at the residential site whereas at the street canyon BBOA concentration was ~~a~~ slightly smaller in daytime, from 6:00 to 17:00, than in the other times of the day. LV-OOA had the largest signal for CO_2^+ and CO^+ at m/z 44 and 28, respectively, and was highly oxygenated with a large O:C. The diurnal pattern of LV-OOA was flat at the residential site but at the street canyon there was a drop in the LV-OOA concentrations from 10:00 to 19:00.

When the number of factors was increased from three to four, LV-OOA was split to LV-OOA and semi-volatile OOA (SV-OOA) at the residential site (Fig. ~~S9a~~S13a). Additionally, the mass contribution of HOA decreased when going from three to four factor solution while the contribution of BBOA remained almost at the same level. In four factor solution, SV-OOA was less oxidized than LV-OOA with the largest signal for $C_2H_3O^+$ at m/z 43. In terms of diurnal pattern, SV-OOA had clearly smaller concentrations from 9:00 to 19:00 at the residential site. Also at the street canyon, the fourth factor was identified as SV-OOA. SV-OOA obtained mass from LV-OOA and BBOA (Fig. ~~S10a~~S14a). Similar to the residential site, SV-OOA had the largest signal for $C_2H_3O^+$ at m/z 43 in the mass spectra and in the diurnal trend a decrease in daytime, however, at the street canyon smaller concentrations in daytime lasted shorter in time (only from 11:00 to 17:00).

In five factor solution, LV-OOA was split into two factors of which one was related to the long-range transported particles (called as LV-OOA-LRT) at the residential site. LV-OOA-LRT had very similar mass spectra to other LV-OOA, but their time series and diurnal trends differed significantly as LV-OOA-LRT was observed mostly at the end of the measurement period in April. LRT particles probably originated from agricultural burning or wildfires since they had a high contribution of organics and BC, however, at the end of the LRT episode, also inorganic species, sulfate, nitrate and ammonium, were mixed with the biomass burning emissions.

At the street canyon, the fifth factor was identified as coffee roastery organic aerosol (CoOA). CoOA contributed only 3 % to the total signal (Fig. ~~S10a~~S14a) but it had a very distinctive mass spectra. The mass spectra of CoOA had pronounced peaks at m/z 55, 67, 82 and 109 corresponding to the HR fragments of $C_3H_5N^+$, $C_3H_3N_2^+$, $C_4H_6N_2^+$ and $C_5H_7N_3^+$, respectively, those fragments being characteristic for caffeine (Carbone et al., 2014). CoOA has been observed earlier in Helsinki at the SMEAR III station with a contribution of 1 % to organics (Timonen et al. 2013). However, the street canyon site utilized in this study was located much closer to the coffee roastery (~600 m north from the roastery) than SMEAR III (~1.5 km northeast from the roastery). The emissions from the coffee roastery were observed in three time periods between 6:00 and 18:00~~-~~ that was presumable as the coffee roastery operated only in daytime.

Regarding six factor solution, SV-OOA was split into two similar factors at the residential site. In seven factor solution, there was an additional factor that contained practically only rBC fragments, and in eight factor solution HOA was split into two identical factors. At the street canyon, six factor solution split LV-OOA. In seven factor solution, another SV-OOA appeared while in eight factor solution HOA was divided. Since the PMF solutions from six to eight factors did not provide any additional information, from now on, only the solutions from three to five factors are investigated in more detail.

BBOA factor was compared with MAs analysed from the 24-hour PM_{10} filter samples collected at the residential site. It was found that for three factor solution the correlations between BBOA and levoglucosan and BBOA and mannosan were weaker than for four and five factor solutions (Fig. ~~S11~~S15). In contrast, for BBOA and galactosan, the correlation was strongest for three factor solution with the Pearson's correlation coefficient (r) decreasing slightly when increasing the number of factors. In terms of the non-refractory species measured by the SP-AMS, sulfate correlated strongest with LV-OOA r increasing significantly going from four to five factors (Fig. ~~S12~~S16). Also nitrate and ammonium had largest r with LV-OOA, but for them, the difference between the number of factors was smaller. Chloride and potassium correlated strongest with BBOA and HOA, the correlation between potassium and BBOA being slightly smaller for three factor solution than for four and five factor solutions. None of the non-refractory species correlated clearly with SV-OOA or LV-OOA-LRT. HOA correlated strongly with NO and NO_x~~-~~, r being larger for four and five factor solutions than for three factor solution.

At the street canyon, sulfate, nitrate and ammonium correlated with LV-OOA with no difference between the number of factors (Fig. ~~S13~~S17). Different from the residential area, chloride and potassium had smallest r with BBOA and HOA. CoOA had a modest correlation with chloride. In terms of nitrogen oxides, HOA had the largest (but moderate) correlation with NO_2. MAs were measured at the street canyon site only every three days and therefore were not compared with BBOA.

The contribution of rBC fragments to the total signal in the mass spectra of the PMF factors is given in Tables S1 and S2. At the residential site, the contribution of rBC was largest to the mass spectra of BBOA in three and four factor solution while in five factor solution the contribution of rBC was largest for LV-OOA. At the street canyon, the contribution of rBC was largest to HOA independent of the number of factors. The contribution of rBC to HOA was more than double at the street canyon compared to that at the residential site. In contrast, the mass spectra of BBOA had several times more rBC at the residential site than at the street canyon. Also the mass spectra of organics in BBOA differed between the residential and street canyon sites as the contribution of $C_2H_4O_2^+$ (at m/z 60) and $C_3H_5O_2^+$ (at m/z 73) was much larger at the residential site compared to the contribution at the street canyon indicating that BBOA at the street canyon site was probably more aged with its mass spectra resembling SOA. That can make the separation of primary and secondary OA factors more complicated at the street canyon site.

The distribution of rBC between the PMF factors is shown in Figs. ~~S9b~~ S13b and S14~~0~~b from three to five factor solutions. Compared to the total mass spectra utilized in the PMF analysis (Organics+rBC), BBOA and HOA had larger contributions to rBC than to Organics+rBC at the residential site. The contribution of BBOA to rBC was smaller in five factor solution than in three and four factor solutions while HOA had the smallest contribution in four factor solution. On the other hand, SV-OOA and LV-OOA and LV-OOA-LRT had smaller contributions to rBC than to Organics+rBC excluding LV-OOA in five factor solution that had larger contribution to rBC than to Organics+rBC. At the street canyon, HOA had larger and BBOA smaller contribution to rBC than to Organics+rBC. For LV-OOA and SV-OOA the contributions to Organics+rBC and rBC were almost equal.

The sum of C_2^+, C_3^+ and C_4^+ fragments included in the PMF input data matrix was compared with the sum of the same fragments found in the PMF solutions at the residential site and street canyon (Fig. ~~S14~~ S18 and S19~~5~~). It can be seen from the figure that for the residential site, the correlation was largest for five factor solution while at the street canyon correlation coefficient was slightly smaller for five factor solution than for three and four factor solutions. Somewhat similar trends were obtained when the sum of C_2^+, C_3^+ and C_4^+ fragments was replaced by HRBC (including all C_x^+ fragments in the mass spectra) calculated in PIKA. In general, the PMF solution was able to explain the majority of the variation of C_2^+, C_3^+ and C_4^+ fragments at the residential site, however, at the street canyon, the difference between the sum of C_2^+, C_3^+ and C_4^+ fragments in PIKA and PMF solution was larger. In general, the unresolved mass (Organics+rBC) was 1.9, 2.2 and 1.6 % at the residential site and 3.6, 3.5, 2.6 % at the street canyon for three, four and five factor solutions, respectively.

PMF solutions from three to five factors were examined for the rotational freedom by varying fpeak and for the accuracy with bootstrapping and multiple seeds. Based on these validation tests, it was found that for the street canyon data, four and five factor solutions did not provide consistent results, especially the contribution of CoOA varied significantly. Therefore, three factor solution was selected to represent the sources of rBC at the street canyon most accurately. For the residential site, five factor solution was chosen as it was found to explain the variation of the rBC sources most realistically.

-Detailed figures on the residuals for the chosen solutions are presented in Figs S20 and S21. For the residential site (five factors), there was some unexplained mass during the daytime and especially in the evening, shown by the diurnal variation of the residuals. That is, however, in line with Frölich et al. (2015) who noticed that in the evening when the concentration of organics was highest the scaled residuals in PMF tended to be slightly larger than at the other times of the day. In terms of mass spectra, the largest residuals were calculated for the CO_2^+, CO^+ and C_3^+ fragments, but relative to the measured signal, they did not stand out in the mass spectra. At the street canyon, there was some unexplained mass during the morning rush hour and evening. The largest absolute residual was calculated for C_3^+ fragment followed by CO_2^+ and CO^+, but similar to the residential site, the residuals for these fragments did not distinguish from the others when the residuals were calculated relative to the measured signal.

For the comparison, PMF was applied also to the organic mass spectra without the C_x fragments included to examine if the rBC fragments affected the PMF solutions. Five factor solution for the residential site and three factor solution for the street canyon data are presented in Fig. ~~S16~~ S22 for organics. Very similar factors were obtained for organics compared to those with Organics+rBC for both data sets (Fig. ~~S17~~ S23 and S25~~19~~). Regarding the time series (Fig. ~~S18~~ S24 and S26~~0~~), only LV-OOA differed slightly when PMF was applied to only organics compared to PMF applied to Organics+rBC at the residential site.

In the following chapters, we discuss only rBC associated with the PMF factors. Therefore, rBC related to BBOA, HOA, LV-OOA, SV-OOA and LV-OOA-LRT factors is hereafter referred as BC_{BBOA}, BC_{HOA}, $BC_{SV\text{-}OOA}$, $BC_{LV\text{-}OOA}$ and $BC_{LV\text{-}OOA\text{-}LRT}$, respectively. For the simplicity, rBC was replaced by BC.

2.3.2 Ångström exponent and aethalometer model

Absorption Ångström exponent values were calculated by using two wavelengths (470 and 950 nm) with the equation:

$$\alpha_{470/950} = -\frac{\ln(\mathrm{b_{abs}}(470\ \mathrm{nm})/\mathrm{b_{abs}}(950\ \mathrm{nm}))}{\ln(470/950)} \qquad (1)$$

where b_{abs} is aerosol light absorption coefficient given by the AE33.

The fraction of wood burning BC (BC_{wb}) was calculated by using the aethalometer model (Sandradewi et al., 2008a; 2008b):

$$\mathrm{BC_{wb}} = \frac{\left(\frac{\mathrm{b_{abs}}(470\ \mathrm{nm}) - \mathrm{b_{abs}}(950\ \mathrm{nm}) * \left(\frac{470}{950}\right)^{-\alpha\mathrm{ff}}}{\left(\frac{470}{950}\right)^{-\alpha\mathrm{wb}} - \left(\frac{470}{950}\right)^{-\alpha\mathrm{ff}}}\right)}{\mathrm{b_{abs}}(950\ \mathrm{nm})} * \mathrm{BC} \qquad (2)$$

Two pairs of Ångström exponent values were utilized to obtain BC associated with fossil fuel (BC_{ff}) and wood burning (BC_{wb}); α_{ff} and α_{wb} of 0.9 and 1.68 (Zotter et al., 2017), and instrument default values α_{ff} and α_{wb} of 1 and 2, respectively. In the previous work of Helin et al. (2018), α values equal to $\alpha_{ff} = 1.10$ and $\alpha_{wb} = 1.60$ at the street canyon and $\alpha_{ff} = 0.95$ and $\alpha_{wb} = 1.60$ at the detached house area were estimated for aerosol in the Helsinki area based on the concurrent levoglucosan analysis. Those values were not utilized in this study as the data of Helin et al. (2018) and this study differed in site locations, measurement year as well as the AE33 tape batch. Additionally, the aim of this study was to select contrasting α_{ff}/α_{wb} pairs to investigate the impact of α_{ff}/α_{wb} values on the BC source apportionment. Same α_{ff}/α_{wb} pairs that were used in this study have also been utilized in Virkkula (2020) that modelled the uncertainties related to the absorption by eBC from fossil fuel and wood burning with a core-shell Mie model.

3 Results and discussion

3.1 Sources of BC at the residential area

The average (±stdev) BC concentration was 0.86 (±1.5) µg m^{-3} at the residential site during the measurements from 15 January to 16 April 2019 (1-hour averaged AE33 data). Regarding the sources of BC, five PMF factors were found to explain the variation of BC at the residential site. On average, the largest fraction of BC was related to biomass burning (BC_{BBOA}; 38 %; Fig. 1) followed by BC associated with LV-OOA ($BC_{LV\text{-}OOA}$; 27 %) and HOA (BC_{HOA}; 17 %) factors. BC attributed to SV-OOA ($BC_{SV\text{-}OOA}$) and LV-OOA-LRT ($BC_{LV\text{-}OOA\text{-}LRT}$) factors had similar contributions (9 %).

BC_{BBOA} originated mostly from local small-scale wood burning. Majority of the houses at the area had at least one fireplace, and since the measurements were carried out during cold season, fireplaces were used frequently in many houses. Specially at the beginning of the measurement campaign, the ambient temperature was low reaching the campaign-minimum of -21 °C (1-hour average) on 22 Jan 2019 (Fig. ~~S21~~S27). During that day, the BC concentration had a campaign-maximum of 24 µg m^{-3} (10-min average) and BC_{BBOA} constituted as much as 80 % of total BC. Besides on 22 Jan, there were several episodes of biomass smokes during the first two weeks of the campaign. On average, the fraction of BC_{BBOA} was 60 % in the first two weeks after which it decreased to 23–37 % in terms of weekly averages (Fig. 1b).

BC_{BBOA} had a clear maximum in the evening between 20:00 and 22:00 but also a small increase in the morning between 9:00 and 10:00 (Fig. 1c). Extensive use of fireplaces in the evening for heating purposes together with heating of sauna stoves was a likely cause of large evening peaks. Also temperature and wind speed typically decreased in the evening (Fig. ~~S22~~S28) causing poor atmospheric dilution. In general, the largest BC_{BBOA} concentrations were observed when the temperature was below -5 °C, but besides that, the temperature-dependency of BC_{BBOA} was small (Fig. ~~S23~~S29). Regarding different days of the week, the contribution of BC_{BBOA} was slightly larger on Saturday than on other days that can be explained by the tradition of heating sauna stoves on Saturday evening.

In the earlier study conducted at the Helsinki residential area (Helin et al., 2018), the average contribution of BC_{wb} to total BC was 46 ± 13 % in winter calculated with the aethalometer model. That is a ~~slightly~~ larger contribution that the campaign-average percentage obtained in this study (38 %), however, it is smaller than the average contribution during the first two weeks of the measurements (60 %). Helin et al. (2018) detected similar diurnal pattern with the BC_{wb} maximum in the evening but in their study also an increase in BC_{ff} was observed in the evening concurrently with BC_{wb}. In other locations in Europe, the contribution of wood burning to BC has been measured to vary in the range of 7–88 % in wintertime (Sandradewi et al., 2008b; Herich et al., 2011; Sciare et al., 2011; Drinovec et al., 2015; Becerril-Valle et al., 2017) the smallest contributions measured typically at urban locations and largest values at rural areas.

BC_{HOA} was mostly associated with vehicle exhaust emissions. BC_{HOA} peaked between 8:00 and 10:00 in the morning and the concentrations started to increase again after 16:00 and stayed elevated over midnight. The morning peak is probably related to the morning rush hour even though there was not much vehicle traffic near the site. However, as mentioned earlier, there were three large roads within ~1 km from the site that could have also caused BC_{HOA}. Elevated BC_{HOA} concentrations in the evening were likely to be related both to the evening traffic and poor atmospheric mixing conditions. Moreover, BC_{HOA} was smaller at weekends than weekdays indicating its origin being mostly in exhaust emissions. In terms of ambient temperature, the largest BC$_{\mathrm{HOA}}$ concentrations were detected with the lowest temperatures, similar to BC$_{\mathrm{BBOA}}$ (Fig. ~~S23~~S29).

BC$_{\mathrm{LV\text{-}OOA}}$ was likely related to regional urban background and/or long-range transported BC as the related PMF factor (LV-OOA) correlated with inorganic species, sulfate, nitrate and ammonium. BC$_{\mathrm{LV\text{-}OOA}}$ concentrations were slightly larger at the beginning of the campaign and the contribution of BC$_{\mathrm{LV\text{-}OOA}}$ to total BC was largest during the third and fourth week of the measurements (Fig. 1b). The diurnal trend of BC$_{\mathrm{LV\text{-}OOA}}$ was very flat with no dependence on the time of the day. Regarding temperature, the largest BC$_{\mathrm{LV\text{-}OOA}}$ concentrations were detected when the ambient temperature was near zero (Fig. ~~23~~S29).

BC$_{\mathrm{LV\text{-}OOA\text{-}LRT}}$ was especially attributed to the long-range transported biomass smokes as BC$_{\mathrm{LV\text{-}OOA\text{-}LRT}}$ peaked in April when two LRT episodes were observed. The first episode lasted almost four days (from 2 to 6 April 2019) while the second episode lasted only slightly longer than one day (from the late evening of 6 April to the early hours of 8 April 2019).- According to the calculated air mass back trajectories (Fig. S30), LRT aerosol arrived in Helsinki from agricultural burning or wildfires in Eastern Europe. During those episodes, BC$_{\mathrm{LV\text{-}OOA\text{-}LRT}}$ composed 50 % of total BC, however, in terms of weekly averages, the largest contribution of BC$_{\mathrm{LV\text{-}OOA\text{-}LRT}}$ was 30 % in week 14 (Fig. 1b). BC$_{\mathrm{LV\text{-}OOA\text{-}LRT}}$ did not display a clear diurnal trend. In terms of ambient temperature, the largest BC$_{\mathrm{LV\text{-}OOA\text{-}LRT}}$ concentrations were observed when the temperature was above zero (Fig. ~~S23~~S29) that was expected as the LRT episodes detected in Finland are mostly related to the transport of warm air masses from south-east to south-west sector (Central or Eastern Europe). It has been shown in earlier studies that BC concentrations are typically 2–4 times larger during the LRT episodes compared to the non-episodic periods (Saarikoski et al., 2007; Saarnio et al., 2010a). LRT episodes observed in Helsinki in April 2019 will be discussed in more detail in another~~the other~~ paper.

BC$_{\mathrm{SV\text{-}OOA}}$ had only a minor (9 %) contribution to total BC at the residential site. In terms of time series, BC$_{\mathrm{SV\text{-}OOA}}$ concentration did not change much during the measurements, however, BC$_{\mathrm{SV\text{-}OOA}}$ concentration was smaller from 9:00 to 21:00 than at the other times of the day. Based on the mass spectra of organics in the SV-OOA factor and its diurnal trend, it can be speculated that BC$_{\mathrm{SV\text{-}OOA}}$ was related to the aging of local traffic and biomass burning emissions. BC$_{\mathrm{SV\text{-}OOA}}$ concentrations did not depend on the ambient temperature (Fig. ~~S23~~S29).

By assuming that BC$_{\mathrm{BBOA}}$ and BC$_{\mathrm{HOA}}$ are locally emitted, the average contribution of local sources to BC was 55 % being slightly larger at the beginning of the campaign (Fig. 2). Remaining BC fractions, BC$_{\mathrm{LV\text{-}OOA}}$, BC$_{\mathrm{LV\text{-}OOA\text{-}LRT}}$ and BC$_{\mathrm{SV\text{-}OOA}}$, are likely to be either related to regional background or LRT. Regional/LRT BC fraction was compared with the BC concentrations measured concurrently at the Luukki regional background site approximately 15 km northwest from the residential site. It can be seen from the timeseries that the sum of BC$_{\mathrm{LV\text{-}OOA}}$, BC$_{\mathrm{LV\text{-}OOA\text{-}LRT}}$ and BC$_{\mathrm{SV\text{-}OOA}}$ measured at the residential site followed closely the timeseries of BC at the background site (Fig. 2). However, at the beginning of the measurements in January 2019, there were some cases when BC was larger at the background site than the sum of BC$_{\mathrm{LV\text{-}OOA}}$, BC$_{\mathrm{LV\text{-}OOA\text{-}LRT}}$ and BC$_{\mathrm{SV\text{-}OOA}}$ at the residential site, probably caused by the local BC emissions at the background site accumulated in the boundary layer due to the temperature inversion.- Although the background site of Luukki is located in a sparsely inhabited area, there are some houses only few hundred meters away from the site, which can have an impact on the measured concentrations.

Regarding the size distributions, BC was typically found at the particle size between 100 and 1000 nm at the residential site (Fig. 3a). The size distribution of BC depended on the main BC source. BC peaked between 200 and 500 nm in the evening, when there was a lot of biomass burning, while at the other times of the day, including morning, BC was detected at the larger particle size with the maximum between 350 and 800 nm. Fig. 3b presents average BC mass size distributions for the periods when BC was impacted by biomass burning (BC_{BBOA} 72 % of BC) and regional background ($BC_{LV\text{-}OOA} + BC_{SV\text{-}OOA}$; 47 % of BC). During the BC_{BBOA} period, the maximum was located at ~300 nm while during the regional background period the maximum was measured at ~550 nm. Note that the total BC concentration was 20 times smaller for the regional background period. During the LRT episode in April, the maximum of the BC size distribution was between that of biomass burning episode and regional background at ~350–450 nm (~~not shown~~Fig. 3b). The size distributions of organics were very similar to those of BC during the three periods (Fig. S31a) indicating that BC was mostly internally mixed with organics.

BC emitted from different sources was also investigated in relation to gaseous CO_2 concentrations measured concurrently at the residential site. From the BC/CO_2 plots it can be noticed that the BC_{HOA} concentration increased clearly when CO_2 increased, however, for the other factors the relationship was less clear (Fig. ~~S24~~S32). The BC-to-CO_2 ratio was investigated in more detail for the local combustion sources, BC_{BBOA} and BC_{HOA}. Background CO_2 concentration, that was defined as the smallest 1 % of the CO_2 concentrations measured at the residential site being equal to 404 ppm, was subtracted from the measured CO_2 concentrations and remaining CO_2 was plotted against BC_{HOA} and BC_{BBOA} concentrations (Fig. 4). Moreover, the data points were classified according to the fraction of BC_{HOA} or BC_{BBOA} in total BC; only the data points when BC_{HOA} or BC_{BBOA} contributed 30–70 % or > 70 % to total BC were selected (30–70 % marked with open circles and > 70 % with closed circles in Fig. 4). For BC_{HOA} the slope was 0.019 $\mu g\ m^{-3}\ ppm^{-1}$ when BC_{HOA} was > 70 % and 0.017 $\mu g\ m^{-3}\ ppm^{-1}$ when the mass fraction of BC_{HOA} was 30–70 %. For BC_{BBOA} the slope was 0.10 $\mu g\ m^{-3}\ ppm^{-1}$ (> 70 % to total BC), which suggests that biomass burning produces approximately five times more BC in relation to CO_2 during biomass burning events compared to engine emissions. However, there was a lot scattering in the BC_{BBOA}-to-CO_2 ratio likely due to the unstable burning conditions in domestic fireplaces that can in turn result in large differences in emitted BC (Heringa et al., 2011; Kortelainen et al., 2018). When converting the slope of BC_{HOA} to the BC emission factor (EF_{BC}) by using a carbon mass fraction (CMF) ratio of CMF_{CO2}/CMF_{fuel} of 3141 g (kg fuel)$^{-1}$ (Enroth at al., 2016), a value equal to 0.03 g $kgfuel^{-1}$ was obtained. That was roughly one fifth of EF_{BC} measured in 2012 in Helsinki at the roadside (Enroth et al., 2016) but it was at the same level with EF_{BC} measured near road in Toronto, Canada in 2016 (Wang et al., 2018). For $BC_{BBOA,}$ EF_{BC} was not calculated as emitted BC and CO_2 depend largely on biomass material burnt as well as the combustion conditions and devices (Savolahti et al., 2016).

3.2 Sources of BC at the street canyon

The average (±stdev) BC concentration at the street canyon in October 2015 was 0.90 (±0.74) $\mu g\ m^{-3}$ for the 1-hour averaged data measured with the AE33. Three PMF factors were found to be related to the sources of BC, BBOA, HOA and LV-OOA, that were similar in mass spectra to those found at the residential site. More than half (57 %) of BC was made of BC_{HOA} at the street canyon, on average (Fig. 5a). Similar to the residential site, BC_{HOA} peaked during morning rush hour (7:00–10:00) and again between 15:00 and 21:00 in the evening (Fig. 5b) indicating that it originated predominantly from vehicle exhaust emissions. Different from the residential site, BC_{HOA} did not remain at the elevated level in night-time as the smallest BC_{HOA} concentrations were detected between 2:00 and 6:00. In the earlier study of Helin et al. (2018), 83–91 % of BC has been associated with fossil fuel combustion at the street canyon in Helsinki by the aethalometer model. BC_{HOA} and BC_{ff} can, however, represent slightly different sources as will be discussed later in Section 3.3. Both the measurements presented in this paper and in Helin et al. (2018) were conducted in 2015–2016. Compared to the situation today, BC related to traffic emissions can be assumed to be smaller than in 2015–2016 as a general declining trend of BC concentrations related to traffic has been presented recently for Helsinki area by Luoma et al. (2021). They found statistically significant decreasing trend in the range of -10.4 – -5.9 % $\mathrm{yr^{-1}}$. The decrease was most noticeable at the traffic sites and particularly during morning rush hour.

The second largest contributor to BC at the street canyon was $\mathrm{BC_{LV\text{-}OOA}}$ (32 %). $\mathrm{BC_{LV\text{-}OOA}}$ did not display a clear diurnal variation. Like at the residential site, $\mathrm{BC_{LV\text{-}OOA}}$ was assumed to be mostly related to regional background or long-range transported BC as the corresponding PMF factor (LV-OOA) correlated with sulfate, nitrate and ammonium. The comparison with the background BC concentrations could not be conducted as there was no BC measurement at the background site in the Helsinki area in 2015. The contribution of $\mathrm{BC_{BBOA}}$ was rather small (11 %) at the street canyon. The measurements at the street canyon were performed in autumn when the ambient temperature was still quite high (an average of 7 °C) so there was no need for the additional heating with wood. Moreover, the street canyon site was located at an urban area surrounded by apartment buildings that did not have fireplaces. In terms of diurnal profiles, $\mathrm{BC_{BBOA}}$ showed larger concentrations in the evening and night.

The mass size distributions of BC are presented in Fig. 5c for two cases; BC was dominated by traffic emissions and BC was mostly related to regional background or LRT. When traffic emissions dominated BC ($\mathrm{BC_{HOA}}$ 80 % of BC), there were two modes of which the first one was located at ~130 nm and the second one at ~300 nm. The mode at ~100–150 nm has been earlier detected for the traffic emissions (Enroth et al., 2016) while the second mode was probably also related to regionally distributed BC or LRT. During the period of regional background or LRT period ($\mathrm{BC_{LV\text{-}OOA}}$ 70 % of BC), there was only one mode that was located at larger particle size (~450 nm) than the second mode for the $\mathrm{BC_{HOA}}$ period. This suggests that $\mathrm{BC_{LV\text{-}OOA}}$ was ~~clearly~~ possibly associated with non-local sources. During the $\mathrm{BC_{LV\text{-}OOA}}$ dominated period, the size distributions of BC was similar to that of organics (Fig. S31b), but in the $\mathrm{BC_{HOA}}$ dominated period, there was slightly more BC in the first mode (at ~130 nm) relative to organics than in the second mode (at ~300 nm).

3.3 Comparison of PMF and aethalometer model source apportionment methods for BC

The source apportionment obtained from the PMF analysis was compared with the absorption properties of particles measured by the AE33. First, an absorption Ångström exponent was calculated for both sites. The α value is typically utilized to characterize different types of aerosols e.g., BC, brown carbon and dust particles, and it has been shown to differ greatly between various emission sources (Kirchstetter et al., 2004; Zotter et al., 2017). The α values measured at the residential and street canyon sites are presented as histograms in Fig. 6. Median α was clearly smaller at the street canyon (1.06) that at the residential site (1.30), however, the shape of the α distribution showed that at the street canyon there were some cases when the α value was larger (~1.2) that the median. Those cases corresponded to large $\mathrm{BC_{BBOA}}$ fraction as the α values calculated specifically for the periods dominated by $\mathrm{BC_{BBOA}}$ or $\mathrm{BC_{HOA}}$ (>50 % of $\mathrm{BC_{BBOA}}$ or $\mathrm{BC_{HOA}}$) were 1.36 and 1.25 at the residential site and 1.24 and 1.12 at the street canyon, respectively. In terms of diurnal variation of the α values, α was smaller in daytime at both sites, the difference between day and night being larger for the street canyon than for the residential area (Fig S33).

The average α values calculated in this study were similar to those found in the earlier study of Helin et al. (2018) in the Helsinki area (1–1.05 and 1.2–1.3 for the street canyon and residential site, respectively). Compared to the α values obtained from the biomass burning emission measurements, Martinsson et al. (2015) have reported the α values between 0.9 and 1.3 for the burning of birch logs in a conventional wood stove, however, α increased to above 2 when fuel was added. For various sauna stoves, α has been measured to be 1.17–1.33, but when wood had high moisture content, α was larger (1.6; Tissari et al., 2019). In ambient measurements, α can be larger than that measured directly from the emission source as α values for biomass burning emissions have been shown to increase due to the atmospheric oxidation processes simulated with a smog chamber (Tasoglou et al., 2017). However, studies have also reported a decrease of α in biomass burning emissions by photooxidation during atmospheric aging (Nicolae et al., 2013, Dasari et al., 2019), which can explain the difference in α if the biomass burning particles are not locally emitted. For the diesel buses, α have been reported to be 0.8–1.2 depending on the driving phase (Helin et al., 2021), while for the motor vehicles emissions measured at a roadway and tunnel, α was in range of 0.6–0.9 (Kirchstetter et al., 2004).

There are several factors that can have an impact on α. One of them is the coating of the BC particles. In this study, the particle coating factor was calculated similar to Drinovec et al. (2017) by summing all the SP-AMS inorganic and organic species (excluding rBC) and dividing it by BC from the AE33. Based on our results, α did not seem to significantly depend on the coating factor, however, there was a tiny increase in α when the coating factor increased (Fig. ~~S25~~S34). Also, the chemical composition of coating was investigated, but the composition did not unambiguously affect α. In general, the coating factor was much larger at the residential site (average coating factor 7.4) compared to that at the street canyon (average coating factor 1.6). It should be noted here that the coating factor calculation had some uncertainties. The assumptions in the coating factor calculations were: (1) CE of 1 for the AMS species, (2) default RIEs for organics and inorganic AMS species, and (3) similar particle size range for the AMS species and BC from the AE33. If the uncertainty of using CE=1 is estimated to be 30 % and the uncertainty of RIEs for each AMS species is 20 %, the total uncertainty due to CE and RIE is ~40 %. The uncertainty in the coating factor due to the different particle sizes measured by the SP-AMS and AE33 is difficult to estimate quantitively. Qualitatively, it can be assumed that the AMS is missing particle mass below <50 nm and therefore the coating factor can be slightly underestimated, especially at the street canyon where there can be small traffic-related particles.

It has been noticed in the earlier studies that also the filter-loading parameter (k) provided by the AE33 can be used to determine particle coating. Drinovec et al. (2017) found a strong anticorrelation between the compensation parameter at 880 nm (k6) and the coating factor suggesting that the coating of BC may be responsible for the decrease of the compensation parameter. In this study, the dependence of k6 on the SP-AMS coating factor was weak. At the residential site, there was a slight negative correlation between k6 and coating factor whereas there was no correlation for the street canyon data (Fig. ~~S25~~S34).

Absorption Ångström exponents can be exploited further for the source apportionment of BC. First, the α values were compared with the fraction of BC_{BBOA} and BC_{HOA} in total BC measured at the residential site (Fig. ~~S26~~S35). It can be seen from the figure that the increasing fraction of BC_{BBOA} somewhat increased the α values whereas the opposite was true for BC_{HOA}. Next, the aethalometer model was applied to the AE33 data sets to calculate the contributions of BC_{ff} and BC_{wb} concentrations. Two pairs of absorption Ångström exponents were used for fossil fuel (α_{ff}) and wood burning (α_{wb}); 1 and 2 (default values from the manufacturer) and 0.9 and 1.68 (Sandadewi et al., 2008b).

In Figure 7 BC_{BBOA} from the PMF analysis was compared with BC_{wb} from the aethalometer model for the residential site data. Biomass burning BC obtained from two source apportionment methods followed very similar time trend, however, BC_{wb} calculated with the α_{ff} and α_{wb} values of 1 and 2, respectively, displayed ~~smaller~~ only half of the values ~~than~~of BC_{BBOA} or BC_{wb} calculated with the α_{ff} and α_{wb} values of 0.9 and 1.68, respectively. The same trend is shown in the scatter plots in Fig. 7b and S36. In terms of diurnal variation (Fig. S37), BC_{BBOA} and BC_{wb} both had a maximum in the afternoon and a second peak in the morning, BC_{BBOA} increasing in both cases slightly later than BC_{wb}. The reason for the delay can speculated to be due to the fact that organics and BC can be emitted at different ratios at different stages of burning (e.g. Kortelainen et al., 2018), the time behavior of BC_{BBOA} being determined by biomass burning organics due to the used PMF method.

~~.~~By converting these values to the percentage of biomass burning BC (BB%), it can be seen that, with the α_{ff} and α_{wb} values of 0.9 and 1.68, the aethalometer model gave larger values than PMF when BB% was small, whereas at larger BB% values, the results from the aethalometer model were smaller than those from PMF. In general, that trend suggests that the aethalometer model produces more constant BB% than PMF and is likely be less sensitive to the changes in the BC sources compared to PMF. Similar observation was done when the diurnal patterns of BB% values ~~BC_{wb} and BC_{BBOA}~~ were compared; BB% from the aethalometer model ~~BC_{wb}~~ had a rather flat diurnal trend whereas BB% from PMF ~~BC_{BBOA}~~ varied more clearly during the course of the day (Fig. S37b). Aethalometer model and PMF results were compared also by adding $BC_{LV\text{-}OOA\text{-}LRT}$ to BB% from PMF (Fig. ~~S27~~S38) since the LRT particles detected in April were likely to be originated from agricultural burning or wildfires. By adding $BC_{LV\text{-}OOA\text{-}LRT}$ to BB% increased small BB% values from PMF, which improved the comparison between PMF and aethalometer model slightly. It should be noted here that a constant α value may not be adapted when there are several BC_{wb} sources at the site, for example local biomass burning and LRT. With the default α_{ff} and α_{wb} values of 1 and 2, BB% from the aethalometer model was much smaller than that from PMF regardless of the PMF factors included in the calculation.

For the street canyon data, BC_{wb} concentrations were mostly larger than BC_{BBOA} concentrations (Fig. 8). In contrast to the residential site, BC_{wb} and BB% values calculated with the aethalometer model by using the α_{ff} and α_{wb} values of 1 and 2 seemed to produce more comparable results with BC_{BBOA} and BB% values from PMF than the α_{ff} and α_{wb} values of 0.9 and 1.68. It should be noted here that the measurement campaign at the street canyon was not optimal for the investigation of biomass combustion because biomass burning was not the major source at the site, and also the measurement campaign was covered only short period of time.

Aethalometer model and PMF source apportionment results can also be compared in terms of BC related to the fossil fuel combustion. At the residential site, BC_{HOA} was much smaller than BC_{ff} calculated with ~~the~~ both sets of α_{ff}/α_{wb} values. This suggests that, besides BC_{HOA}, the regionally distributed BC (mostly $BC_{LV\text{-}OOA}$) originates largely from the fossil fuel combustion at the residential site. Also at the street canyon, BC_{HOA} was much smaller than BC_{ff} from the aethalometer model with both the sets of α_{ff}/α_{wb} values. Exceptions were the cases when the BC concentrations were large and the contributions of both BC_{ff} and BC_{HOA} were close to 100 % indicating that BC originated probably mostly from diesel vehicles. However, the diurnal pattern of BC_{ff} followed that of BC_{HOA} and NO_x well showing both the morning and evening rush hours (Fig. ~~S28~~S39). When $BC_{LV\text{-}OOA}$ was added to the fossil fuel fraction, PMF and BC_{ff} (with both the α_{ff}/α_{wb} values) were closer to each other. That suggests that also at the street canyon $BC_{LV\text{-}OOA}$ was mostly related to the fossil fuel combustion. Here BC_{ff} refers to the fossil fuel combustion, however, it is likely to also include BC from biofuels e.g. biodiesel and ethanol.

4 Conclusions

This study investigated the sources of BC at two contrasting locations; at the residential area in winter- and springtime and at the street canyon in autumn. It was shown that PMF applied to the SP-AMS data is a powerful tool to determine the main sources of BC at urban environments. PMF analysis revealed that the largest fraction of BC originated from local biomass burning at the residential site (average 38 %) whereas the main source of BC was vehicular exhaust emissions at the street canyon (57 %). At both sites, a considerable fraction of BC consisted of regional urban background or long-range transported BC indicated by the high oxidation state of organics related to those PMF factors as well as the comparison with BC detected at the background site outside of Helsinki. On average, the total BC concentration was very similar at the two sites (~0.9 µg m^{-3}). When comparing the sites, it should be remembered that the measurements were conducted at different years (residential site in 2019 and street canyon in 2015) that may also impact the source contributions. For example, Luoma et al. (2021) have shown that BC related to traffic has decreased in Helsinki area in recent years, which may overrate traffic related BC at the street canyon relative to year 2019.

The source had an impact on the detected size of BC particles. BC from traffic was found at the particle size of ~100–150 nm whereas BC from biomass combustion was observed at ~300 nm. BC was located at the largest particle size (~500–600 nm) when the impact of the local sources was small, however, during an intense LRT episode, the maximum of BC size distribution was shifted to a slightly smaller size (~400 nm). Moreover, the coating thickness of BC particles was very different at the residential and street canyon sites. There was much thicker coating at the residential site (average coating factor 7.4) than at the street canyon (average coating factor 1.6). The size of the BC core as well as coating thickness and composition have significant impacts on BC climate and health effects.

Comparison of the PMF results with the BC source apportionment from the aethalometer model indicated that several PMF factors can be related to wood burning and fossil fuel fractions obtained from the aethalometer model. Moreover, PMF was able to separate additionally local, regional background and LRT contributions. In general, the aethalometer model presented smaller variation for the sources within a day than PMF being less responsive to the fast changes in the BC sources at the site. It is also possible that the aethalometer model was not able to distinguish between as many sources as PMF due to similar optical properties of the BC sources. It should be noted here also that a constant α value may not be adapted when there are several biomass burning sources at the site, for example local biomass burning and LRT.~~.~~

The results of this study improve the understanding of the limitations and validity of the aethalometer model for BC source apportionment in different kinds of environment. Based on the results of this study, the aethalometer model can provide estimates for the fractions of BC related to biomass combustion and fossil fuel combustion. The aethalometer model is most suitable for the environment that is mainly impacted either by wood combustion or vehicle emissions, but if there are several sources, the results from the aethalometer model are more difficult to interpret. The advantage of the aethalometer model is that BC_{ff} and BC_{wb} can be calculated from the data of a reasonably simple BC instrument. However, the uncertainty of the model is related to the unique set of α_{ff}/α_{wb}

values needed for each measurement site. Additionally, as the aethalometer relies on the filter-based measurement technique, the filter batch used in the AE33 may affect the results.

In terms of PMF applied to the SP-AMS data, the largest uncertainty is related to the expertise and experience of the PMF user. The selection of the accurate number of factors as well as the validation of data can be challenging and provide questionable results. Moreover, the quantification of the rBC by the SP-AMS can be tricky as the detection of rBC is strongly influenced by the overlap of particle and laser beams. Due to the much lower detection efficiency of rBC relative to organics, the PMF method for the SP-AMS data is likely to be more suitable for urban environments with more BC in relation to organics than in remote areas.

Overall, the results of this study provide novel information on local, regional and remote sources of BC in urban environments. Although the measurements were carried out only in Helsinki, the results and the applied measurement and data analysis methods are applicable to the other areas as well. The BC source apportionment results are highly valuable for the modelers when calculating the climate and air quality impact of BC as well as for the authorities when directing the emission legislation and emission mitigation actions.

Data availability. The data shown in the paper is available on request from corresponding author.

Author contribution. SS, JVN, TR and HT designed the experiments and SS, JVN and MA performed the measurements. SS, JVN, MA, LP and AK performed the data analysis. SS wrote the first version of the manuscript, but all authors participated in the writing process. HT, TR, LP, JVN and SS contributed to the acquisition of funding for the study.

Competing interests. The authors declare that they have no conflict of interest.

Acknowledgements. This work was supported by Business Finland, HSY, Valmet Technologies, Vaisala, Tampere City, Pegasor, Dekati, AX-Consulting, AGCO Power, Airmodus, and SSAB Europe in the project Black Carbon Footprint (grant no. 1462/31/2019, 530/31/2019). We also acknowledge funding from the European Regional Development Fund, Urban innovative actions initiative (HOPE; Healthy Outdoor Premises for Everyone, project nro: UIA03-240), Academy of Finland Flagship funding Atmosphere and Climate Competence Center, ACCC (grant no. 337552, 337549) and COST–COLOSSAL (CA16109).

References

Alfarra, M.R., Prevot, A.S.H., Szidat, S., Sandradewi, J., Weimer, S., Lanz, V.A., Schreiber, D., Mohr, M., and Baltensperger, U.: Identification of the mass spectral signature of organic aerosols from wood burning emissions, Environ. Sci. Technol., 41, 5770–5777, https://doi.org/10.1021/es062289b, 2007.

AMAP, 2015. Summary for Policy-makers: Arctic Climate Issues 2015. Arctic Monitoring and Assessment Programme (AMAP), Oslo, Norway. 16 pp.

Barreira, L. M. F., Helin, A., Aurela, M., Teinilä, K., Friman, M., Kangas, L., Niemi, J. V., Portin, H., Kousa, A., Pirjola, L., Rönkkö, T., Saarikoski, S., and Timonen, H.: In-depth characterization of submicron particulate matter inter-annual variations at a street canyon site in Northern Europe, Atmos. Chem. Phys., 21, 6297–6314, https://doi.org/10.5194/acp-21-6297-2021, 2021.~~ Discuss., https://doi.org/10.5194/acp-2020-908, in review, 2020.~~

Becerril-Valle, M., Coz, E., Prévôt, A., Močnik, G., Pandis, S., de la Campa, A. S., Alastuey, A., Díaz, E., Pérez, R., and Artíñano, B., Characterization of atmospheric black carbon and co-pollutants in urban and rural areas of Spain. Atmos. Environ., 169, 36–53, https://doi.org/10.1016/j.atmosenv.2017.09.014, 2017.

Bibi, Z., Coe, H., Brooks, J., Williams, P. I., Reyes-Villegas, E., Priestley, M., Percival, C., and Allan, J. D.: Technical Note: A new approach to discriminate different black carbon sources by utilising fullerenes and metals in Positive Matrix Factorisation analysis of High-Resolution Soot Particle Aerosol Mass Spectrometer data, Atmos. Chem. Phys. Discuss., https://doi.org/10.5194/acp-2020-890, in review, 2020.

Bond, T. C., Doherty, S. J., Fahey, D. W., Forster, P. M., Berntsen, T., DeAngelo, B. J., Flanner, M. G., Ghan, S., Kärcher, B., Koch, D., Kinne, S., Kondo, Y., Quinn, P. K., Sarofim, M. C., Schultz, M. G., Schulz, M., Venkataraman, C., Zhang, H., Zhang, S., Bellouin, N., Guttikunda, S. K., Hopke, P. K., Jacobson, M. Z., Kaiser, J. W., Klimont, Z., Lohmann, U., Schwarz, J. P., Shindell, D., Storelvmo, T., Warren, S. G., and Zender, C. S.: Bounding the role of black carbon in the climate system: A scientific assessment, J. Geophys. Res., 118, 5380–5552, https://doi.org/10.1002/jgrd.50171, 2013.

Carbone, S., Aurela, M., Saarnio, K., Saarikoski, S., Frey, A., Timonen, H., Sueper, D., Ulbrich, I., Jimenez, J.-L., Kulmala, M., Worsnop D., and Hillamo, R.: Wintertime aerosol chemistry in sub-arctic urban air, Aerosol Sci. Technol., 48, 312–322, https://doi.org/10.1080/02786826.2013.875115, 2014.

Carbone, S., Timonen, H., Rostedt, A., Happonen, M., Rönkkö, T., Keskinen, J., Ristimäki, J., Korpi, H., Artaxo, P., Canagaratna, M., Worsnop, D., Canonaco, F., Prévôt, A.S.H., Hillamo, R., and Saarikoski, S.: Distinguishing fuel and lubricating oil combustion products in diesel engine exhaust particles, Aerosol Sci. Technol., https://doi.org/10.1080/02786826.2019.1584389, 2019.

Chen, L.-W. A., Watson, J. G.. Chow, J. C., Green, M. C., Inouye, D., Dick, K.: Wintertime particulate pollution episodes in an urban valley of the Western US: a case study, Atmos. Chem. Phys., 12, 10051–10064, https://doi.org/10.5194/acp-12-10051-2012, 2012.

Cooper, J. A., and Watson, J. G.: Receptor Oriented Methods of Air Particulate Source Apportionment, J. Air Pollut. Control Assoc., 30, 1116–1125, https://doi.org/10.1080/00022470.1980.10465157, 1980.

Corbin, J. C., Sierau, B., Gysel, M., Laborde, M., Keller, A., Kim, J., Petzold, A., Onasch, T. B., Lohmann, U., and Mensah, A. A.: Mass spectrometry of refractory black carbon particles from six sources: carbon-cluster and oxygenated ions, Atmos. Chem. Phys., 14, 2591–2603, https://doi.org/10.5194/acp-14-2591-2014, 2014.

Dasari, S., Andersson, A., Bikkina, S., Holmstrand, H., Budhavant, K., Satheesh, S., Asmi, E., Kesti, J., Backman, J., Salam, A., Bisht, D. S., Tiwari, S., Hameed, Z., Gustafsson, Ö.: Photochemical degradation affects the light absorption of water-soluble brown carbon in the South Asian outflow. Sci. Adv., 5, eaau8066, https://doi.org/10.1126/sciadv.aau8066, 2019.

Drinovec, L., Gregorič, A., Zotter, P., Wolf, R., Bruns, E. A., Prévôt, A. S. H., Petit, J.-E., Favez, O., Sciare, J., Arnold, I. J., Chakrabarty, R. K., Moosmüller, H., Filep, A., and Močnik, G.: The filter-loading effect by ambient aerosols in filter absorption photometers depends on the coating of the sampled particles, Atmos. Meas. Tech., 10, 1043–1059, https://doi.org/10.5194/amt-10-1043-2017, 2017.

Drinovec, L., Močnik, G., Zotter, P., Prévôt, A., Ruckstuhl, C., Coz, E., Rupakheti, M., Sciare, J., Müller, T., and Wiedensohler, A.: The" dual-spot" Aethalometer: an improved measurement of aerosol black carbon with real-time loading compensation, Atmos. Meas. Tech., 8, 1965–1979, https://doi.org/10.5194/amt-8-1965-2015, 2015.

~~Engel-Cox, J., and Weber, S. A.: Compilation and Assessment of Recent Positive Matrix Factorization and UNMIX Receptor Model Studies on Fine Particulate Matter Source Apportionment for the Eastern United States, J. Air Waste Manage., 57, 1307–1316, doi:10.3155/1047-3289.57.11.1307, 2007.~~

Enroth, J., Saarikoski, S., Niemi, J. V., Kousa, A., Ježek, I., Močnik, G., Carbone, S., Kuuluvainen, H., Rönkkö, T., Hillamo, R., and Pirjola, L.: Chemical and physical characterization of traffic particles in four different highway environments in the Helsinki metropolitan area, Atmos. Chem. Phys., 16, 5497–5512, https://doi.org/10.5194/acp-16-5497-2016, 2016.

Friedlander, S.K.: Chemical Element Balances and Identification of Air Pollution Sources, Environ. Sci. Technol., 7, 235–240, https://doi.org/10.1021/es60075a005, 1973.

Fröhlich, R., Crenn, V., Setyan, A., Belis, C. A., Canonaco, F., Favez, O., Riffault, V., Slowik, J. G., Aas, W., Aijälä, M., Alastuey, A., Artiñano, B., Bonnaire, N., Bozzetti, C., Bressi, M., Carbone, C., Coz, E., Croteau, P. L., Cubison, M. J., Esser-Gietl, J. K., Green, D. C., Gros, V., Heikkinen, L., Herrmann, H., Jayne, J. T., Lunder, C. R., Minguillón, M. C., Močnik, G., O'Dowd, C. D., Ovadnevaite, J., Petralia, E., Poulain, L., Priestman, M., Ripoll, A., Sarda-Estève, R., Wiedensohler, A., Baltensperger, U., Sciare, J., and Prévôt, A. S. H.: ACTRIS ACSM intercomparison – Part 2: Intercomparison of ME-2 organic source apportionment results from 15 individual, co-located aerosol mass spectrometers, Atmos. Meas. Tech., 8, 2555–2576, https://doi.org/10.5194/amt-8-2555-2015, 2015.

Gyawali, M., Arnott, W., Lewis, K., and Moosmüller, H.: In situ aerosol optics in Reno, NV, USA during and after the summer 2008 California wildfires and the influence of absorbing and non-absorbing organic coatings on spectral light absorption, Atmos. Chem. Phys., 9, 8007–8015, https://doi.org/10.5194/acp-9-8007-2009, 2009.

Hansen, J., and Nazarenko, L.: Soot climate forcing via snow and ice albedos, PNAS, 101, 423–428, https://doi.org/10.1073/pnas.2237157100, 2004.

Healy, R., Sofowote, U., Su, Y., Debosz, J., Noble, M., Jeong, C.-H., Wang, J., Hilker, N., Evans, G., and Doerksen, G.: Ambient measurements and source apportionment of fossil fuel and biomass burning black carbon in Ontario, Atmos. Environ., 161, 34–47, https://doi.org/10.1016/j.atmosenv.2017.04.034, 2017.

Helin, A., Niemi, J. V., Virkkula, A., Pirjola, L., Teinilä, K., Backman, J., Aurela, M., Saarikoski, S., Rönkkö, T., Asmi, E., and Timonen, H.: Characteristics and source apportionment of black carbon in the Helsinki metropolitan area, Finland, Atmos. Environ., 190, 87–98, https://doi.org/10.1016/j.atmosenv.2018.07.022, 2018.

Helin, A., Virkkula, A., Backman, J., Pirjola, L., Sippula, O., Aakko-Saksa, P., Väätäinen, S., Mylläri, F., Järvinen, A., Bloss, M., Aurela, M., Jakobi, G., Karjalainen, P., Zimmermann, R., Jokiniemi, J., Saarikoski, S., Tissari, J., Rönkkö, T., Niemi, J. V., Timonen, H.: Variation of Absorption Ångström Exponent in Aerosols from Different Emission Sources, ~~Accepted to~~ J.~~ournal of~~ Geophys.~~ical~~ Res.~~earch~~, 126, https://doi.org/10.1029/2020JD034094, 2021.

Herich, H., Hueglin, C., and Buchmann, B.: A 2.5 year's source apportionment study of black carbon from wood burning and fossil fuel combustion at urban and rural sites in Switzerland, Atmos. Meas. Tech., 4, 1409–1420, https://doi.org/10.5194/amt-4-1409-2011, 2011.

Hietikko, R., Kuuluvainen, H., Harrison, R. M., Portin, H., Timonen, H., Niemi, J. V., and Rönkkö, T.: Diurnal variation of nanocluster aerosol concentrations and emission factors in a street canyon, Atmos. Environ., 189, 98–106, https://doi.org/10.1016/j.atmosenv.2018.06.031, 2018.

Huang L., Brook J.B., Zhang W., Li S.M., Graham L., Ernst D., Chiculescu A., and Lu G.: Stable isotope measurements of carbon fractions (OC/EC) in airborne particulate: A new dimension for source characterization and apportionment, Atmos. Environ., 40, 2690–2705, 2006.

Ikeda, K., Tanimoto, H., Sugita, T., Akiyoshi, H., Kanaya, Y., Zhu, C., and Taketani, F.: Tagged tracer simulations of black carbon in the Arctic: transport, source contributions, and budget, Atmos. Chem. Phys., 17, 10515–10533, https://doi.org/10.5194/acp-17-10515-2017, 2017.

IPCC, 2014. In: Pachauri, R.K., Meyer, L.A. (Eds.), Climate Change 2014: Synthesis Report. Contribution of Working Groups I, II and III to the Fifth Assessment Report of the Intergovernmental Panel on Climate Change [Core Writing Team, Geneva, Switzerland, 151 pp.

Heringa, M. F., DeCarlo, P. F., Chirico, R., Tritscher, T., Dommen, J., Weingartner, E., Richter, R., Wehrle, G., Prévôt, A. S. H., and Baltensperger, U.: Investigations of primary and secondary particulate matter of different wood combustion appliances with a high-resolution time-of-flight aerosol mass spectrometer, Atmos. Chem. Phys., 11, 5945–5957, https://doi.org/10.5194/acp-11-5945-2011, 2011.

Janssen, N. A. H., Hoek, G., Simic-Lawson, M., Fischer, P., van Bree, L., ten Brink, H., Keuken, M., Atkinson, R.W., Anderson, H.R., Brunekreef, B., and Cassee, F.R.: Black carbon as an additional indicator of the adverse health effects of airborne particles compared with PM_{10} and $PM_{2.5}$, Environ. Health Perspect., 119, 1691–1699, doi: 10.1289/ehp.1003369, 2011.

Jayne, J. T., Leard, D. C., Zhang, X., Davidovits, P., Smith, K. A., Kolb, C. E., and Worsnop, D. R.: Development of an Aerosol Mass Spectrometer for Size and Composition Analysis of Submicron Particles, Aerosol Sci. Technol., 33, 49–70, https://doi.org/10.1080/027868200410840, 2000.

Järvinen, A., Timonen, H., Karjalainen, P., Bloss, M., Simonen, P., Saarikoski, S., Kuuluvainen, H., Kalliokoski, J., DalMaso, M., Niemi, J., Keskinen, J., and Rönkkö, T.: Particle emissions of Euro VI, EEV and retrofitted EEV city buses in real traffic, Environ. Pollut., 250, 708–716, https://doi.org/10.1016/j.envpol.2019.04.033, 2019.

Kirchstetter, T.W., Novakov, T., and Hobbs, P.V.: Evidence that the spectral dependence of light absorption by aerosols is affected by organic carbon, J. Geophys. Res. Atmos., 109, https://doi.org/10.1029/2004JD004999, 2004.

Klimont, Z., Kupiainen, K., Heyes, C., Purohit, P., Cofala, J., Rafaj, P., Borken-Kleefeld, J., and Schöpp, W.: Global anthropogenic emissions of particulate matter including black carbon, Atmos. Chem. Phys., 17, 8681–8723, https://doi.org/10.5194/acp-17-8681-2017, 2017.

Kortelainen, M., Jokiniemi, J., Tiitta, P., Tissari, J., Lamberg, H., Leskinen, J., Grigonyte-Lopez Rodriguez, J., Koponen, H., Antikainen, S., Nuutinen, I., Zimmermann, R., and Sippula, O.: Time-resolved chemical composition of small-scale batch combustion emissions from various wood species, Fuel, 233, 224–236, https://doi.org/10.1016/j.fuel.2018.06.056, 2018.

Kukkonen, J., López-Aparicio, S., Segersson, D., Geels, G., Kangas, L., Kauhaniemi, M., Maragkidou, A., Jensen, A., Assmuth, T., Karppinen, A., Sofiev, M., Hellén, H., Riikonen, K., Nikmo, J., Kousa, A., Niemi, J. V., Karvosenoja, N., Sousa Santos, G., Sundvor, I., Im, U., Christensen, J. H., Nielsen, O.-K., Plejdrup, M. S., Nøjgaard, J. K., Omstedt, G., Andersson, C., Forsberg, B., and Brandt, J.: The influence of residential wood combustion on the concentrations of $PM_{2.5}$ in four Nordic cities, Atmos. Chem. Phys., 20, 4333–4365, https://doi.org/10.5194/acp-20-4333-2020, 2020.

Kuula, J., Friman, M., Helin, A., Niemi, J. V., Aurela, M., Timonen, H., and Saarikoski, S.: Utilization of scattering and absorption-based particulate matter sensors in the environment impacted by residential wood combustion, J. Aerosol Sci., 15, https://doi.org/10.1016/j.jaerosci.2020.105671, 2020.

Lack, D., and Cappa, C.: Impact of brown and clear carbon on light absorption enhancement, single scatter albedo and absorption wavelength dependence of black carbon, Atmos. Chem. Phys., 10, 4207–4220, https://doi.org/10.5194/acp-10-4207-2010, 2010.

Lack, D., and Langridge, J.: On the attribution of black and brown carbon light absorption using the Ångström exponent, Atmos. Chem. Phys. 13, 10535–10543, https://doi.org/10.5194/acp-13-10535-2013, 2013.

Laskin, A., Laskin, J., and Nizkorodov, S.A.: Chemistry of atmospheric brown carbon. Chem. Rev., 115, 4335–4382, https://doi.org/10.1021/cr5006167, 2015.

Luoma, K., Niemi, J. V., Aurela, M., Fung, P. L., Helin, A., Hussein, T., Kangas, L., Kousa, A., Rönkkö, T., Timonen, H., Virkkula, A., and Petäjä, T.: Spatiotemporal variation and trends in equivalent black carbon in the Helsinki metropolitan area in Finland, Atmos. Chem. Phys., 21, 1173–1189, https://doi.org/10.5194/acp-21-1173-2021, 2021.

Martinsson, J., Eriksson, A. C., Elbæk Nielsen, I., Berg Malmborg, V., Ahlberg, E., Andersen, C., Lindgre, R., Nyström, R., Nordin, E. Z., Brune, W. H., Svenningsson, B., Swietlicki, E., Boman, C., and Pagels, J. H.: Impacts of Combustion Conditions and Photochemical Processing on the Light Absorption of Biomass Combustion Aerosol, Environ. Sci. Technol., 49, 14663−14671, https://doi.org/10.1021/acs.est.5b03205, 2015.

Middlebrook, A. M., Bahreini, R., Jiménez, J. L., and Canagaratna, M. R.: Evaluation of composition-dependent collection efficiencies for the Aerodyne aerosol mass spectrometer using field data, Aerosol Sci. Technol. 46, 258–271, 2012.

Nicolae, D., Nemuc, A., Müller, D., Talianu, C., Vasilescu, J., Belegante, L., Kolgotin, A.: Characterization of fresh and aged biomass burning events using multiwavelength Raman lidar and mass spectrometry. J. Geophys. Res., 118, 2956–2965, https://doi.org/10.1002/jgrd.50324, 2013.

Niemi, J. V., Saarikoski, S., Aurela, M., Tervahattu, H., Hillamo, R., Westphale, D. L., Aarnio, P., Koskentalo, T., Makkonen, U., Vehkamäki, H., and Kulmala, M.: Long-range transport episodes of fine particles in southern Finland during 1999–2007, Atmos. Environ., 43, 1255–1264, https://doi.org/10.1016/j.atmosenv.2008.11.022, 2009.

Ohtonen, K., Kaski, N., and Niemi, J.: Tulisijojen käyttö ja päästöt pääkaupunkiseudulla vuonna 2018, HSY:n julkaisuja 1/2020, ISSN 978-952-7146-47-7, https://julkaisu.hsy.fi/tulisijojen-kaytto-ja-paastot-paakaupunkiseudulla-vuonna-2018.pdf, 2020.

Onasch, T. B., Fortner, E. C., Trimborn, A. M., Lambe, A. T., Tiwari, A. J., Marr, L. C., Corbin, J. C., Mensah, A. A., Williams, L. R., Davidovits, P., and Worsnop, D. R.: Investigations of SP-AMS Carbon Ion Distributions as a Function of Refractory Black Carbon Particle Type, Aerosol Sci. Technol., 49, 409–422, https://doi.org/10.1080/02786826.2015.1039959, 2015.

Onasch, T. B., Trimborn, A., Fortner, E. C., Jayne, J. T., Kok, G. L., Williams, L. R., Davidovits, P., and Worsnop, D. R.: Soot particle aerosol mass spectrometer: Development, validation, and initial application, Aerosol Sci. Technol., 46, 804–817, https://doi.org/10.1080/02786826.2012.663948, 2012.

Paatero, P., and Tapper, U.: Positive matrix factorization – A nonnegative factor model with optimal utilization of error- estimates of data values. Environmetrics 5, 111–126, https://doi.org/10.1002/env.3170050203, 1994.

Paatero, P.: Least squares formulation of robust non-negative factor analysis, Chemometr. Intell. Lab., 37, 23–35, https://doi.org/10.1016/S0169-7439(96)00044-5, 1997.

Pirjola, L., Dittrich, A., Niemi, J. V., Saarikoski, S., Timonen, H., Kuuluvainen, H., Järvinen, A., Kousa, A., Rönkkö, T., and Hillamo, R., Physical and chemical characterization of real-world particle number and mass emissions from city buses in Finland, Environ. Sci. Technol., 50, https://doi.org/10.1021/acs.est.5b04105, 294−304.

Rivellini, L.-H., Adam, M. G., Kasthuriarachchi, N., and Lee, A. K. Y.: Characterization of carbonaceous aerosols in Singapore: insight from black carbon fragments and trace metal ions detected by a soot particle aerosol mass spectrometer, Atmos. Chem. Phys., 20, 5977–5993, https://doi.org/10.5194/acp-20-5977-2020, 2020.

Saarikoski, S., Salo, L., Bloss, M., Alanen, J., Teinilä, K., Reyes, F., Vázquez, Y., Keskinen, J., Oyola, P., Rönkkö, T., and Timonen. H.: Sources and Characteristics of Particulate Matter at Five Locations in an Underground Mine, Aerosol Air Qual. Res. 19, 2613–2624, https://doi.org/10.4209/aaqr.2019.03.0118, 2019.

Saarikoski, S., Sillanpää, M., Sofiev, M., Timonen, H., Saarnio, K., Teinilä, K., Karppinen, A., Kukkonen, J., and Hillamo, R.: Chemical composition of aerosols during a major biomass burning episode over northern Europe in spring 2006: experimental and modelling assessments, Atmos. Environ., 41, 3577–3589, https://doi.org/10.1016/j.atmosenv.2006.12.053, 2007.

Saarnio, K., Aurela, M., Timonen, H., Saarikoski, S., Teinilä, K., Mäkelä, T., Sofiev, M., Koskinen, J., Aalto, P. P., Kulmala, M., Kukkonen, J., and Hillamo, R.: Chemical composition of fine particles in fresh smoke plumes from boreal wild-land fires in Europe, Sci. Total Environ., 408, 2527–2542, https://doi.org/10.1016/j.scitotenv.2010.03.010, 2010a.

Saarnio, K., Teinilä, K., Aurela, M., Timonen, H., and Hillamo, R.: High-performance anion-exchange chromatography-mass spectrometry method for determination of levoglucosan, mannosan and galactosan in atmospheric fine particulate matter, Anal. Bioanal. Chem., 398, 2253–2264, https://doi.org/10.1007/s00216-010-4151-4, 2010b.

Sandradewi, J., Prévôt, A., Weingartner, E., Schmidhauser, R., Gysel, M., and Baltensperger, U.: A study of wood burning and traffic aerosols in an Alpine valley using a multi-wavelength Aethalometer, Atmos. Environ., 42, 101–112, https://doi.org/10.1016/j.atmosenv.2007.09.034, 2008a.

Sandradewi, J., Prévôt, A. S., Szidat, S., Perron, N., Alfarra, M. R., Lanz, V. A., Weingartner, E., and Baltensperger, U.: Using aerosol light absorption measurements for the quantitative determination of wood burning and traffic emission contributions to particulate matter, Environ. Sci. Technol., 42, 3316–3323, https://doi.org/10.1021/es702253m, 2008b.

Savolahti, M., Karvosenoja, N., Tissari, J., Kupiainen, K., Sippula, O., and Jokiniemi, J.: Black carbon and fine particle emissions in Finnish residential wood combustion: Emission projections, reduction measures and the impact of combustion practices, Atmos. Environ., 140, 495–505, https://doi.org/10.1016/j.atmosenv.2016.06.023, 2016.

Segersson, D., Eneroth, K., Gidhagen, L., Johansson, C., Omstedt, G., Engström Nylen, A., and Forsberg, B.: Health impact of PM_{10}, $PM_{2.5}$ and black carbon exposure due to different source sectors in Stockholm, Gothenburg and Umea, Sweden, Int. J. Res. Public Health, 14, 742, https://doi.org/10.3390/ijerph14070742, 2017.

Sciare, J., d'Argouges, O., Sarda-Estève, R., Gaimoz, C., Dolgorouky, C., Bonnaire, N., Favez, O., Bonsang, B., and Gros, V.: Large contribution of water-insoluble secondary organic aerosols in the region of Paris (France) during wintertime, J. Geophys. Res., 116, D22, https://doi.org/10.1029/2011JD015756, 2011.

Szidat S., Jenk T.M., Gäggeler H.W., Synal H.-A., Fisseha R., Baltensberger U., Kalberer M., Samburova V., Wacker L., Saurer M., Schwikowski M., and Hajdas I.: Source apportionment of aerosols by ^{14}C measurements in different carbonaceous particle fractions, Radiocarbon, 46, 475–484, https://doi.org/10.1017/S0033822200039783, 2004.

Tasoglou, A., Saliba, G., Subramanian, R., and Pandis, S. N.: Absorption of chemically aged biomass burning carbonaceous aerosol, J. Aerosol Sci., 2017, 113, 141–152, https://doi.org/10.1016/j.jaerosci.2017.07.011, 2017.

Timonen, H., Carbone, S., Aurela, M., Saarnio, K., Saarikoski, S., Ng, N. L., Canagaratna, M. R., Kulmala, M. Kerminen, V.-M., Worsnop, D. R., and Hillamo, R.: Characteristics, sources and water-solubility of ambient submicron organic aerosol in springtime in Helsinki, Finland, J. Aerosol Sci., 56, 61–77, https://doi.org/10.1016/j.jaerosci.2012.06.005, 2013.

Tissari, J., Väätäinen, S., Leskinen, J., Savolahti, M., Lamberg, H., Kortelainen, M., Karvosenoja, N., and Sippula, O.: Fine Particle Emissions from Sauna Stoves: Effects of Combustion Appliance and Fuel, and Implications for the Finnish Emission Inventory, Atmosphere, 10, 775; doi:10.3390/atmos10120775, 2019.

Ulbrich, I. M., Canagaratna, M. R., Zhang, Q., Worsnop, D. R., and Jimenez, J. L.: Interpretation of organic components from Positive Matrix Factorization of aerosol mass spectrometric data, Atmos. Chem. Phys., 9, 2891–2918, https://doi.org/10.5194/acp-9-2891-2009, 2009.

Virkkula, A.: Modeled source apportionment of black carbon particles coated with a light-scattering shell, Atmos. Meas. Tech. Discuss., https://doi.org/10.5194/amt-2020-438, in review, 2020.

Wang, Y., Hopke, P.K., Rattigan, O.V., Xia, X., Chalupa, D.C., and Utell, M.J.: Characterization of residential wood combustion particles using the two-wavelength aethalometer, Environ. Sci. Technol., 45, 7387–7393, https://doi.org/10.1021/es2013984, 2011a.

Wang, J. M., Jeong, C.-H., Hilker, N., Shairsingh, K. K., Healy, R. M., Sofowote, U., Debosz, J., Su, Y., McGaughey, M., Doerksen, G., Munoz, T., White, L., Herod, D., and Evans, G. J.: Near-Road Air Pollutant Measurements: Accounting for Inter-Site Variability Using Emission Factors, Environ. Sci. Technol., 52, 16, 9495–9504,
https://doi.org/10.1021/acs.est.8b01914, 2018.

Wang, Y., Hopke, P. K., Rattigan, O. V., and Zhu, Y.: Characterization of ambient black carbon and wood burning particles in two urban areas, J. Environ. Monit., 13, 1919–1926, DOI:10.1039/c1em10117j, 2011b.

WHO, 2012. Health Effects of Black Carbon. World Health Organization, Regional Office for Europe, Copenhagen.

Yoon, S., Fairley, D., Barrett, T. E., and Sheesley, R. J.: Biomass and fossil fuel combustion contributions to elemental carbon across the San Francisco Bay Area, Atmos. Environ., 195, 229-242, https://doi.org/10.1016/j.atmosenv.2018.09.050, 2018.

Yttri, K. E., Simpson, D., Stenström, K., Puxbaum, H., Svendby, T.: Source apportionment of the carbonaceous aerosol in Norway – quantitative estimates based on 14C, thermal-optical and organic tracer analysis, Atmos. Chem. Phys., 11, 9375–9394, https://doi.org/10.5194/acp-11-9375-2011, 2011.

Zotter, P., Herich, H., Gysel, M., El-Haddad, I., Zhang, Y., Močnik, G., Hüglin, C., Baltensperger, U., Szidat, S., and Prévôt, A.S.H.: Evaluation of the absorption Ångström exponents for traffic and wood burning in the Aethalometer-based source apportionment using radiocarbon measurements of ambient aerosol, Atmos. Chem. Phys., 17, 4229–4249, https://doi.org/10.5194/acp-17-4229-2017, 2017.

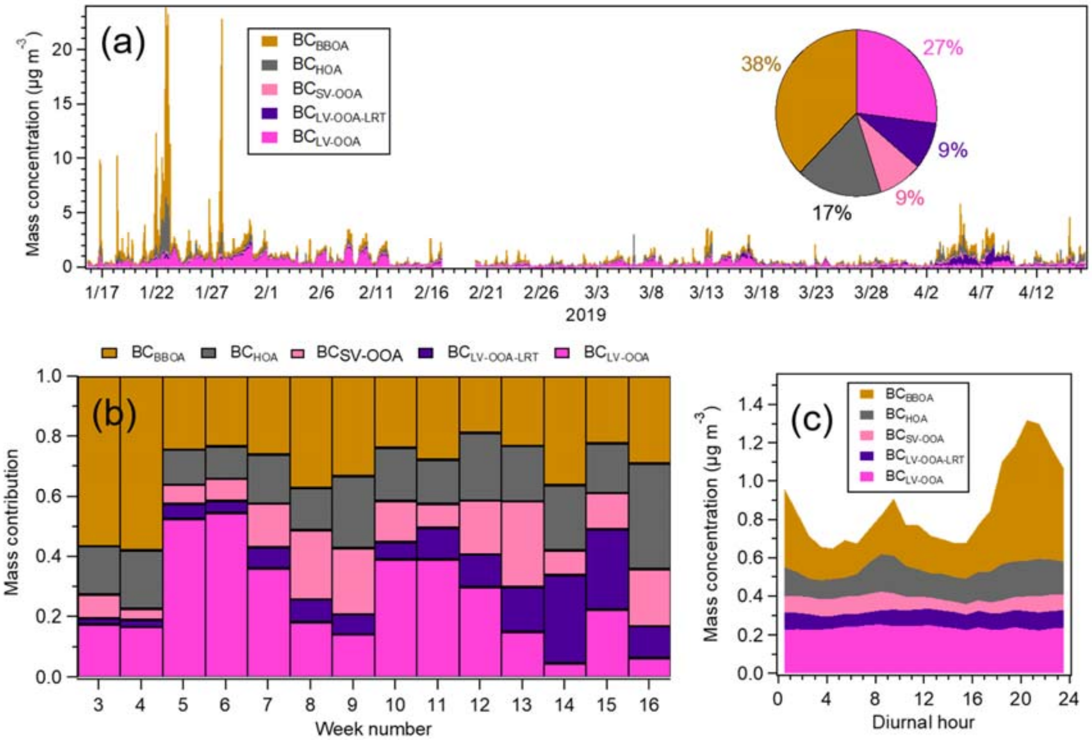

Figure 1. Source apportionment of BC at the residential site by using PMF for the SP-AMS data. Time series with average contributions (a), weekly average contributions (b), and diurnal variations (c). Time series in (a) are presented with 10-min time-resolution.

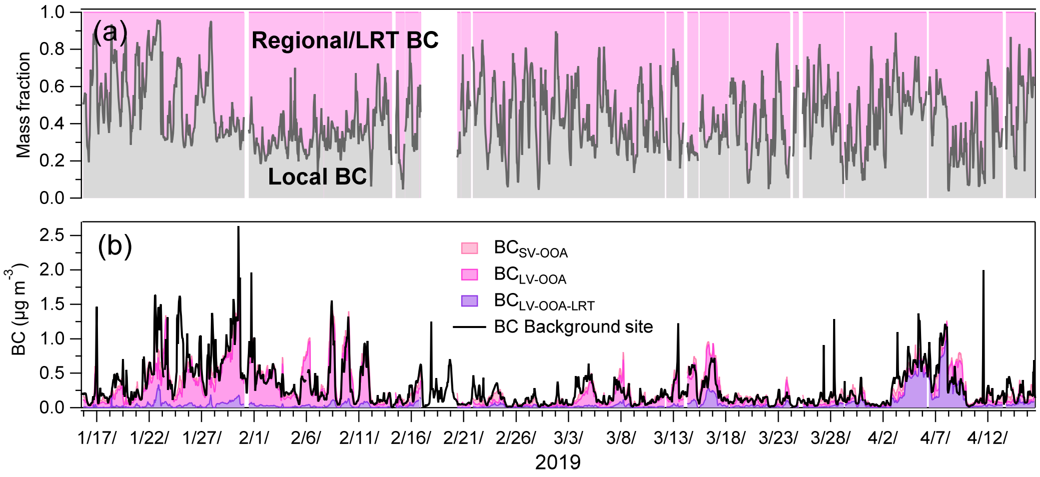

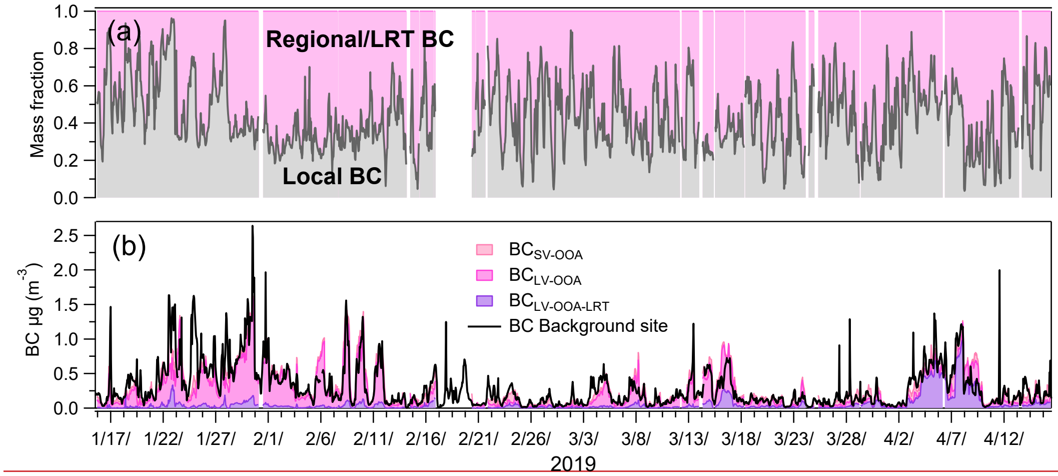

Figure 2. Regional or long-range transported vs. local BC at the residential area. The distribution of BC to local and regional/LRT BC at the residential site (a), and the time series of $BC_{LV\text{-}OOA}$, $BC_{LV\text{-}OOA\text{-}LRT}$ and $BC_{SV\text{-}OOA}$ at the residential site (stacked) compared with total BC at the background site (b).

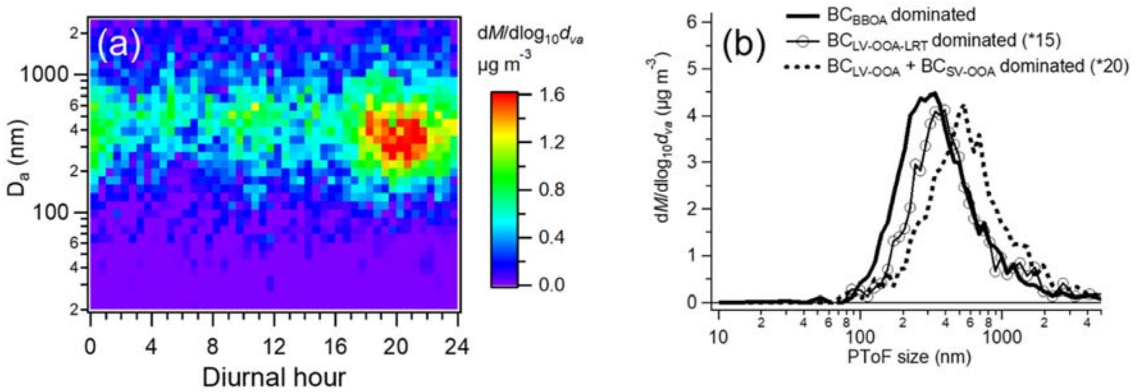

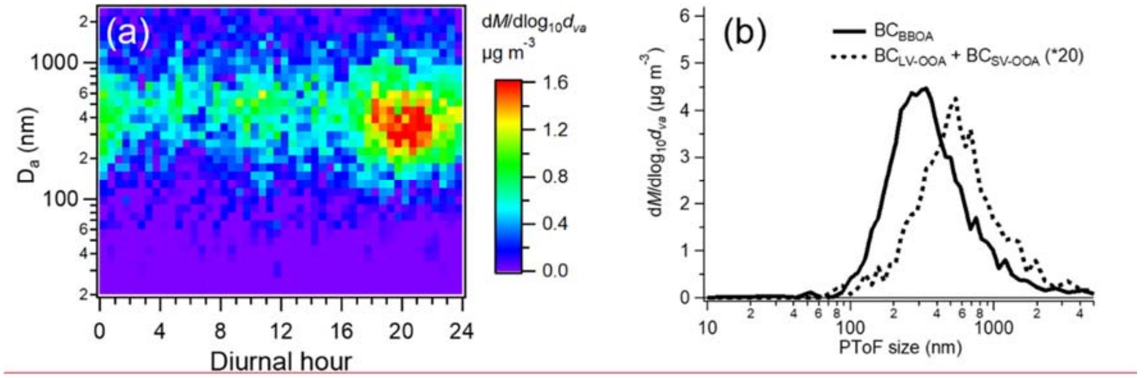

Figure 3. Mass size distribution of BC at the residential area. The evolution of mass size distributions during the day (a) and the examples of the mass size distribution during the periods when BC_{BBOA}~~-~~, $BC_{LV\text{-}OOA\text{-}LRT}$ or the sum of $BC_{LV\text{-}OOA}$ $BC_{SV\text{-}OOA}$ dominated total BC concentration (b). Data for (a) was collected from 16 Jan to 28 Feb 2019 when there were intensive biomass burning episodes. BC_{BBOA} period in (b) was measured on 22 Jan 2019 from 19:45 to 23:30, $BC_{LV\text{-}OOA\text{-}LRT}$ period from 4 April 2019 at 3:45 to 5 April 2019 at 23:30, and ~~and~~ $BC_{LV\text{-}OOA}$ + ~~-~~$BC_{SV\text{-}OOA}$ period from 17 March to 1 April 2019.

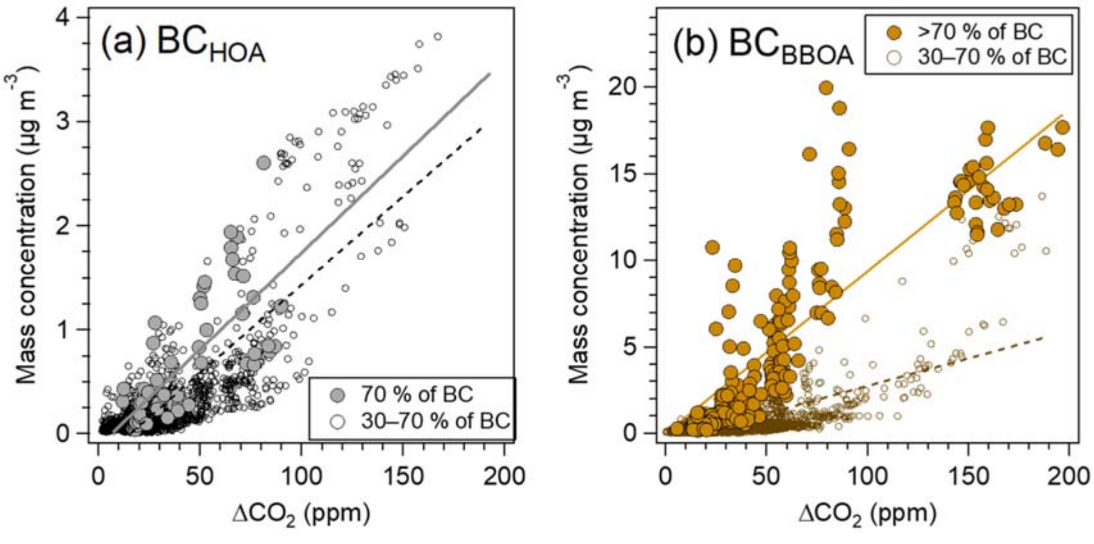

Figure 4. The relationship between BC_{HOA} and BC_{BBOA} to CO_2 concentrations at the residential site. BC_{HOA} (a) and BC_{BBOA} (b) vs. ΔCO_2 concentrations. ΔCO_2 was calculated as $CO_{2(}$measured) - CO_2(background) and

CO_2(background) was 404 ppm. The slopes were 0.019 and 0.017 (HOA) and 0.10 and 0.032 (BBOA) for > 70 % and 30–70 % of BC, respectively. 10-minute average values.

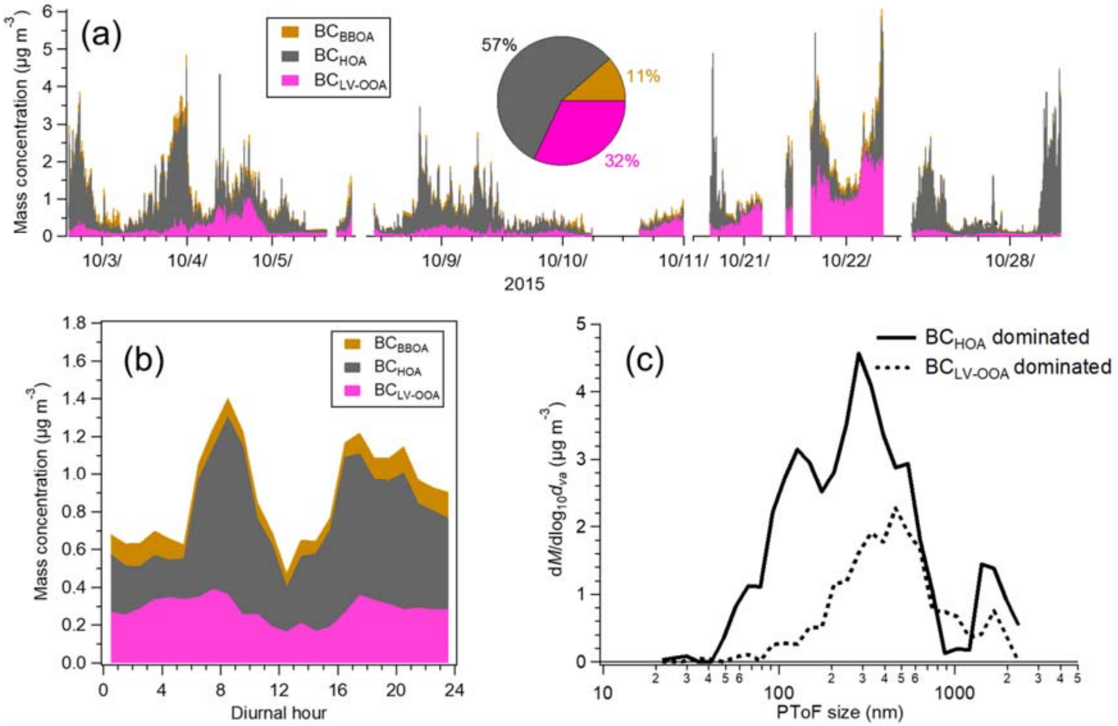

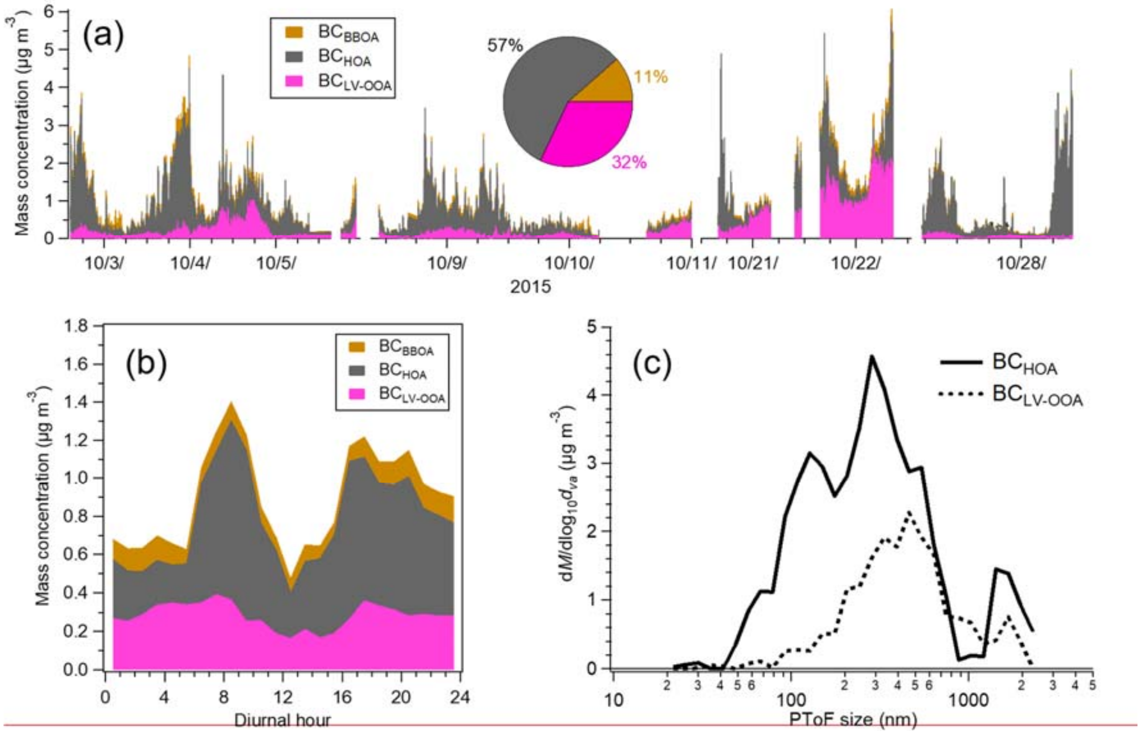

Figure 5. Source apportionment of BC by using PMF and size distributions for the SP-AMS data at the street canyon. Time series with average contributions (a) and diurnal variations (b) of the BC fractions, and the size distributions when BC_{HOA} and OOA fraction dominated (3 October 2015, 18:30 to 23:55 and 21 October 2015, 20:00 to 22 October 2015, 4:00, respectively). Time series in (a) are presented with 5-min time-resolution.

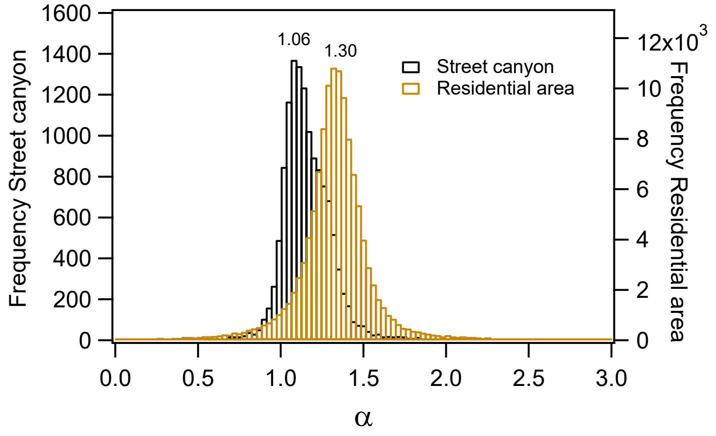

Figure 6. Absorption Ångström exponents calculated for the street canyon and residential area data. Histograms for 1-min resolution data.

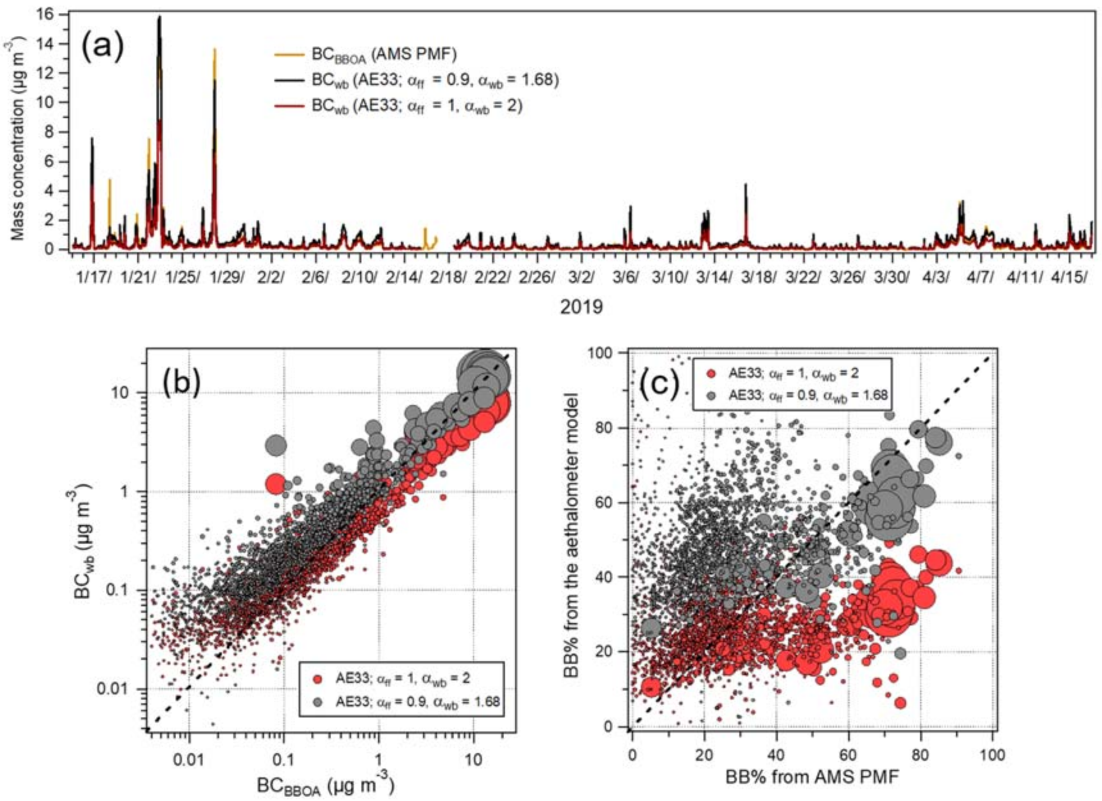

Figure 7. Comparison of AMS-PMF with the aethalometer model source apportionment for BC at the residential site. Time series (a), the scatter plot of BC_{wb} and BC_{BBOA} concentrations (b) and BB% (c). BC_{wb} and BB% with the aethalometer model was calculated by using $\alpha_{ff} = 0.9$ and $\alpha_{wb} = 1.68$, and $\alpha_{ff} = 1$ and $\alpha_{wb} = 2$. 1-hour time-resolution. Marker size in (b) and (c) illustrates the concentration of total BC. Dotted line in (b) and (c) shows 1:1 line.

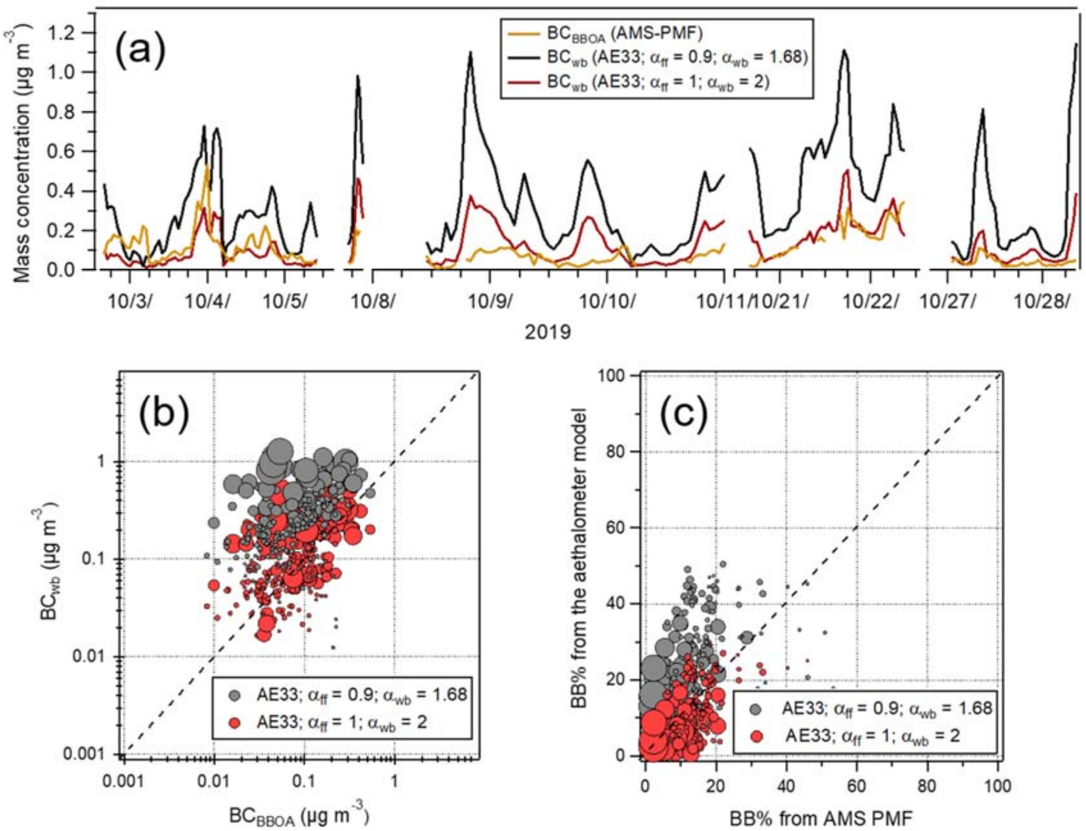

Figure 8. Comparison of AMS-PMF with the aethalometer model source apportionment for BC at the street canyon. Time series (a), the scatter plot of BC$_{wb}$ and BC$_{BBOA}$ concentrations (b) and BB% (c). BB% with the aethalometer model was calculated by using α_{ff} = 0.9 and α_{wb} = 1.68, and α_{ff} = 1 and α_{wb} = 2. 1-hour time-resolution. Marker size in (b) and (c) illustrates the concentration of total BC. Dotted line in (b) and (c) shows 1:1 line.